AD-A088 522 COLORADO STATE UNIV FORT COLLINS DEPT OF CHEMISTRY F/G 7/4
VIBRONIC ASSIGNMENTS AND VIBRONIC COUPLING IN THE 1E' STATE OF--ETC(U)
AUG 80 J D WEBB, K M SWIFT, E R BERNSTEIN N00014-79-C-0647
UNCLASSIFIED TR-1-2469 NL

1 OF 1
AD A
0885..

END
DATE
FILMED
9-80
DTIC

(12)

OFFICE OF NAVAL RESEARCH
Contract N00014-79-C-0647

TECHNICAL REPORT No. 1-2469

"VIBRONIC ASSIGNMENTS AND VIBRONIC COUPLING IN THE ${}^1E''$ STATE OF SYM-TRIAZINE BY TWO PHOTON SPECTROSCOPY"

by

J. D. WEBB, K. M. SWIFT, and E. R. BERNSTEIN

Prepared for Publication in
The Journal of Chemical Physics

Department of Chemistry
Colorado State University
Fort Collins, Colorado 80523

11 August 1980

Reproduction in whole or in part is permitted for
any purpose of the United States Government.

Approved for Public Release; Distribution Unlimited.

UNCLASSIFIED

SECURITY CLASSIFICATION OF THIS PAGE (When Data Entered)

REPORT DOCUMENTATION PAGE

READ INSTRUCTIONS BEFORE COMPLETING FORM

1. REPORT NUMBER Technical Report No. 1-2469

2. GOVT ACCESSION NO. AD-A088 522

3. RECIPIENT'S CATALOG NUMBER (14) TR-1-2469

4. TITLE (and Subtitle) (6) "VIBRONIC ASSIGNMENTS AND VIBRONIC COUPLING IN THE $^1E''$ STATE OF SYM-TRIAZINE BY TWO PHOTON SPECTROSCOPY"

5. TYPE OF REPORT & PERIOD COVERED TECHNICAL REPORT (17)

6. PERFORMING ORG. REPORT NUMBER

7. AUTHOR(s) (10) J.D. Webb, K. M. Swift [redacted] E. R. Bernstein

8. CONTRACT OR GRANT NUMBER(s) N00014-79-C-0647 (15)

9. PERFORMING ORGANIZATION NAME AND ADDRESS

Department of Chemistry
Colorado State University
Fort Collins, Colorado 80523

10. PROGRAM ELEMENT, PROJECT, TASK AREA & WORK UNIT NUMBERS (12) 61

11. CONTROLLING OFFICE NAME AND ADDRESS

Office of Naval Research
Arlington, Virginia 22217

12. REPORT DATE (11) Aug[redacted]980

13. NUMBER OF PAGES 57

14. MONITORING AGENCY NAME & ADDRESS (if different from Controlling Office)

15. SECURITY CLASS. (of this report) UNCLASSIFIED

15a. DECLASSIFICATION/DOWNGRADING SCHEDULE

16. DISTRIBUTION STATEMENT (of this Report)

Approved for Public Release; Distribution Unlimited.

17. DISTRIBUTION STATEMENT (of the abstract entered in Block 20, if different from Report)

18. SUPPLEMENTARY NOTES

19. KEY WORDS (Continue on reverse side if necessary and identify by block number)

sym-triazine; two photon spectroscopy; vibronic coupling; excited state; photoacoustic detection; rotational contour analysis; polarization; Jahn-Teller coupling; single vibronic level fluorescence (SVLF) spectra.

20. ABSTRACT (Continue on reverse side if necessary and identify by block number)

Two photon photoacoustically detected spectra are reported for the first excited singlet state $^1E'$ of sym-triazine in the gas phase. The origin has been positively identified as of E' symmetry through contour calculations and hot band observations. The excited state absorption is dominated by a highly irregular [illegible] progression. These observations include: 6_0^1 (A_1'') ~0 cm^{-1}, approx.

DD FORM 1 JAN 73 1473 EDITION OF 1 NOV 65 IS OBSOLETE

UNCLASSIFIED 409992

I. INTRODUCTION

The molecular properties of sym-triazine ($C_3N_3H_3$) have been of considerable continued interest over the past 25 years.[1-16] Optical spectroscopy has been one of the major ongoing efforts in the study of geometry, excited state energy levels, and dynamics of sym-triazine. There are a number of reasons for this. First, sym-triazine is of high molecular symmetry (D_{3h}) with relatively few atoms, thereby reducing its vibrational and electronic complexity to some extent. Second, it is the only small aromatic molecular system with a degenerate, readily accessible, first excited state. Third, vibronic coupling in this system can be quite extensive; both intrastate (Jahn Teller - JT) and interstate (pseudo-Jahn Teller - PJT) couplings are potentially large. Fourth, the molecule is of considerable biological interest, particularly as a model system for many other nitrogen heterocycles. Fifth, radiationless relaxation from the lowest singlet and triplet states is fast and for the most part poorly understood. In view of the foregoing, it was thought that the new technique of two photon spectroscopy would be an excellent method for the further study of this system.

The first optical spectrum of triazine vapor located a broad, intense transition at 272 nm,[1] which was assigned by solvent shift studies as $n \rightarrow \pi^*$ (A_2'').[2,4] Subsequent analysis of the hot band region showed many of the weak, sharp features were associated with an electric dipole (one photon) forbidden E" state.[8] Low temperature crystal studies have confirmed these assignments.[9-13] Single vibronic level fluorescence (SVLF) spectra are also in agreement with this conclusion.[14]

The ${}^1E'' \leftarrow {}^1A_1'$ transition is two photon allowed and it was felt two photon spectroscopic experiments would be an obvious way to

20. ABSTRACT (continued)

6^1_0 (E") ~227 cm^{-1}, 6^2_0 (E") ~556 cm^{-1}, 6^3_0 (E") ~693 cm^{-1}, and possibly 6^4_0(E") [8^1_0(E") or 19^1_0(E")] ~836 cm^{-1} above the ^{1}E" origin. The one photon observed 6^1_0 (A''_2) and 6^2_0 (A''_2) bands at 677 cm^{-1} and 1176 cm^{-1} respectively, fit in well with these assignments. These observations are strongly supported by a Jahn Teller calculation which predicts: little coupling between the A''_2 and E" electronic manifolds; a large quadratic coupling and a small linear coupling in the E" manifold; and a quenched angular momentum in this state. Good agreement is shown to exist between one photon and two photon spectroscopic observations and the calculations.

A'_2 E'

increase our understanding of the excited state, its geometry, vibronic coupling, and relaxation processes. However, since triazine is known to emit only weakly, two photon excitation experiments employing conventional detection techniques (fluorescence) were not expected to be successful. Photoacoustic detection does, however, provide a straightforward,reliable method for obtaining the desired gas phase spectra. We have recently reported preliminary results of two photon experiments on triazine detected by means of the photoacoustic effect and by fluorescence from photochemically generated cyanyl (CN).[17] This paper presents more complete results and a more detailed discussion of our findings and conclusions. (It should be noted that some of the previous assignments have been changed in the present paper due to new experimental and theoretical findings but that the general conclusions remain unaltered.)

Vibronic assignments are made with the help of rotational contour analysis and polarization studies.[18,19] The isotropic part of the Q branch of a totally symmetric vibronic state will be observed in absorption if viewed in linearly polarized light but will not be observed if circularly polarized light is employed. The polarization behavior of hot bands can be used to imply the vibronic symmetry of the corresponding cold bands (Sect.IV). With these methods, combined with other standard techniques of spectroscopic analysis, it has been possible to give a unique assignment for most of the major features of the $^1E'' \leftarrow {}^1A_1'$ absorption spectrum.

The presentation is organized as follows. In Section II we present background information on triazine and Jahn Teller (JT) coupling. Section III describes experimental details of the two photon photoacoustic and fluorescence apparatus employed.In Section IV we present experimental results. Rotational contour and vibronic coupling calculations used to understand the spectroscopic assignments are given in Section V. Manifestations of the JT effect in the $^1E''$ state are discussed in Section VI. Our findings are summarized in Section VII.

II. BACKGROUND

Early spectroscopic studies of sym-triazine[1,2,4] suggested the energy level diagram and excited state symmetries shown in Figure 1. The intense portion of the 272 nm band observed in one photon spectra is seen to be the one photon allowed A_2'' electronic state. However, Brinen's identification of the electronic origin was subsequently shown to be incorrect.[4,8] Ground state vibrational frequencies and rotational constants were determined by infrared and Raman spectroscopy[3,5]; these are given in Table I. Ground state geometry was determined to be planar, and of D_{3h} symmetry.

Udagawa's partial rotational contour analysis of one of the weak, sharp bands on the low energy side of the 272 nm band indicated that triazine is planar (or at least nearly so) in its lowest excited singlet state.[7] Fisher and Small were able to assign some of the sharp, weak transitions on the low energy side of the 272 nm band as being due to an E" electronic state by consideration of vibronic selection rules and by identification of some vibronically allowed hot bands.[8] They realized that JT coupling within the E" manifold was possible but they were unable to find definitive evidence for it. A summary of their vibrational assignments is given in Table II.

Knight and Parmenter's SVLF data[14] on sym-triazine support these E" electronic and 6_0^1 (A_2'') vibronic assignments. Only ν_6 appears to be active in the SLVF spectra, indicating that a model in which a single vibrational mode vibronically couples to the E" electronic state is reasonable. This situation is to be contrasted to that found for benzene[20] and transition metal hexafluorides.[21-23] Furthermore, the SVLF intensity pattern for the

ν_6 progression $[I(6^1_2) > I(6^1_4) >> I(6^1_3) \sim I(6^1_5) \sim I(6^1_6)]$ indicates that quadratic JT (QJT) coupling is more important than linear JT (LJT) coupling. If LJT vibronic coupling is dominant, the pumped level [the n=1 $\nu_6(A''_2)$ vibronic component in the $^1E''$ excited state] will be mixed with all other $\nu_6(A''_2)$ components ($n \geq 2$) in the $^1E''$ electronic state, since LJT coupling has the selection rule $\Delta n = \pm 1$. In order for emission to occur, the electric dipole allowed $^1A''_2$ electronic state about 1500 cm^{-1} above the $^1E''$ origin must be mixed into the pumped level as well. LPJT coupling will mix $\nu_6(A''_2)$ components ($n = 0,2,3...$) of the $^1A''_2$ electronic state into the pumped level with the selection rule $\Delta n = \pm 1$. Since the pumped level has contained in it all ν_6 (A''_2) levels of the $^1E''$ electronic state (due to LJT coupling), LPJT coupling will mix in all $\nu_6(A''_2)$ components of the $^1A''_2$ electronic state to some extent. Note that this coupling omits ν_6 $n = 1$ of $^1A''_2$ which is of E'' vibronic symmetry. QJT coupling, on the other hand, will mix ν_6 components of the $^1E''$ electronic state according to the selection rule $\Delta n = 0, \pm 2$. Thus, the $n = 1$ $\nu_6(A''_2)$ level which is being pumped will contain the other ν_6 (A''_2) components of the $^1E''$ electronic state with odd n. LPJT coupling will mix in even $\nu_6(A''_2)$ components from the $^1A''_2$ electronic state according to the LPJT selection rule $\Delta n = \pm 1$. The intensity of the emission progression $6^1_n(A''_2)$ $(^1E'' \rightarrow {}^1A'_1)$ will be proportional to $\langle {}^1A''_2\, n' | \underline{r} | {}^1A'_1 n \rangle = \langle {}^1A''_2 | \underline{r} | {}^1A'_1 \rangle \langle n' | n \rangle$ which, in the absence of large Franck-Condon shifts, will be greatest for $n' = n$. With LJT coupling mixing $n = 0,2,3,4...$ $\nu_6(A''_2)$ levels of the $^1A''_2$ electronic state into the pumped level, emission should occur to ν_6 levels $n = 0,2,3,4...$ of the ground state. With QJT coupling dominant, the pumped level contains only even n $\nu_6(A''_2)$ components from the $^1A''_2$ electronic state, so emission will occur to even n ν_6 levels in the ground electronic state, thus predicting $I(6^1_3) \sim 0$ and $I(6^1_4)$ large in agreement with the experimental SVLF data. Figure 2 illustrates this effect and how it comes about.

Barnard has carried out high resolution one photon studies of sym-triazine vapor and has done a careful rotational contour analysis.[24] He concluded that electronic angular momentum in the $^1E''$ state is largely quenched ($-0.2<\zeta_e<0.1$). A summary of his other results is included in Table II. An important conclusion from this work is that the 6^2_0 (A''_2) state is only 499 cm^{-1} above the 6^1_0 (A''_2) at 677 cm^{-1}. Such an energy level pattern is predicted by QJT calculations but never by LJT calculations.

The above discussion intimates that the QJT vibronic coupling is important in the E" electronic state of sym-triazine. Previous theoretical investigations of a QJT coupling have shown that it can be more influential in a given circumstance than might be obvious intuitively.[21-23] Some vibronic levels are effected by QJT coupling in first order perturbation theory whereas LJT coupling effects vibronic levels only in second order perturbation theory. A large quadratic JT effect is present in ReF_6 [21] and IrF_6 [22]. In addition, calculations for these molecules which allowed simultaneous JT coupling in two modes led to quite different results than if the two modes were considered separately.

III. EXPERIMENTAL

Synthesis of h_3- and d_3- sym-triazine samples used in this study is described in references 13 and 25. Additional purification steps such as vacuum distillation, fusion with potassium, and distillation through molecular sieve were carried out in a grease-free vacuum system.

Initial two photon photoacoustic experiments were performed in a sample cell with windows sealed with lightly greased O-rings. It was found that HCN appeared as a decomposition product in such a cell. HCN evolution was monitored photoacoustically (one photon absorption) by observing the fifth overtone of the carbon-hydrogen stretch ($\nu_3 = 3312\ \mathrm{cm}^{-1}$ and $5\nu_3 = 15552\ \mathrm{cm}^{-1}$) which appears fortuitously in the midst of the two photon triazine spectrum. Subsequently, all two photon gas phase cells had windows sealed with indium gaskets; to the limit of our detection ability no HCN is produced in these new cells. However, decomposition is a problem in these experiments nonetheless, as triazine is apparently photodecomposed by an n photon process that is, in any event, two photon resonant. This photochemical process yields CN radicals. CN is detected photoelectrically by monitoring B → X emission in the near ultraviolet, as cyanyl is produced in its excited state. CN is also observed in two photon absorption B ← X followed by emission. The overall process for this photochemistry is described as follows:

$$C_3N_3H_3 \xrightarrow{nh\nu} CN^* + \text{other products} \rightarrow CN + h\nu'$$

$$CN + 2\,h\nu'' \rightarrow CN^* \rightarrow CN + h\nu'.$$

[illegible] two photon absorption is not observed photoacoustically, due either to high quantum yield for emission or low concentration of total photoproducts. CN production involves a two photon resonant triazine process and, with the exception of the readily identified CN absorption ($B(\nu=3) \leftarrow X$), CN fluorescence gives the same triazine line shapes and positions as does the photoacoustically detected spectrum. Some variations in relative intensities of vibronic features have been previously noted,[17] however.

All features observed in the two photon photoacoustically detected spectrum are due only to sym-triazine. This is confirmed by the existence of hot bands separated from cold bands by triazine ground state frequencies. Also, the d_3- triazine origin is blue-shifted by over 100 cm^{-1} while most of the vibrational intervals are almost unchanged.

The experimental arrangement of the two photon photoacoustic apparatus is depicted in Fig.3. The tunable laser for these experiments is a Nd/YAG pumped dye laser (Quanta-Ray DCR-1 & PDL) with an output of 2MWatts over the range 6200-6600 Å using DCM dye. The laser beam is focused in front of a 1" condenser microphone (B&K 4145) mounted in a high vacuum stainless steel cell. A unique feature of this cell design is that a Teflon cup has been mounted on the microphone body in order to enhance signals and reduce background; the best signal occurs for the situation in which the distance between the microphone diaphragm and the end plate of the cup is as small as possible. Apparently two factors are important: focus should be as close to the diaphragm as possible, and the shock wave reflected from the cup should reach the diaphragm while it is still deformed from the initial shock wave. This latter situation insures better signal integration.[26]

Other important cell design features are: absence of grease or epoxy; metal (Cu) flange seals and indium window seals; metal-ceramic feedthrough for microphone electrical connections; and Brewster ouput window of glass-blown quartz and molybdenum sealed. The angled output window eliminates background signals from reflected laser light impinging on the microphone assembly. An angled input window is less necessary and makes polarization experiments difficult.

The microphone signal is amplified (PAR 114/118 amplifier) and is processed by a boxcar integrator (PAR 164/162) (Channel A). The laser power level is monitored by a pyroelectric power meter (Molectron) and processed in the second (B) channel of the boxcar. The two signals are subsequently ratioed (A/B^2) to compensate for pulse-to-pulse variations and the power curve of the dye laser. Wavelength calibration is achieved by splitting off a small fraction of the dye laser beam and using the optogalvanic effect in a standard Fe-Ne hollow cathode lamp to observe well known atomic resonances. Circularly polarized light was produced in a Fresnel rhomb. Hot band experiments were performed at 100°C by heating the cell with a heating tape. Signal to noise ratio for these experiments was about a factor of two to three lower than for room temperature experiments due to depleted ground state population, convection currents in the cell, and increased microphone noise.

Two photon emission excitation experiments were also attempted (both fluorescence and phosphorescence). The experimental arrangement is similar to the above except a photomultiplier tube (RCA 8850) with appropriate filters was used as a detector. Pulses from the 8850 were fed into the boxcar integrator directly. At 10 Torr of sym-triazine vapor, no triazine emission was detected. However, emission from CN was observed, as previously described, and since it is two photon triazine resonant, the absorption could be followed with the $B \rightarrow X$ CN emission. Even at 0.1 Torr only weak CN emission could be detected from the sample.

IV. EXPERIMENTAL RESULTS

Two photon photoacoustic spectroscopic data for h_3- and d_3-triazine are found in Table III and representative survey spectra and individual band contours can be found in Figures 4-9. The first step in assigning the spectrum is to determine the excited state vibronic symmetry for each of the bands. Rotational contour simulation can often associate a unique ΔK selection rule with a given contour, which immediately gives the vibronic symmetry (see Table IV).[27] This method gives the symmetry of the lowest energy cold band as E". Such an assignment is supported by the presence of a polarized hot band at $-346\ cm^{-1}$. This frequency is close to the ground state value for ν''_{16} (e"). The transition assignment $^1E'' \leftarrow {}^1E''$ (e" $^1A'_1$) (16^0_1) explains both the location and polarization behavior of the band (Table IV). The lowest cold band is thus identified as an E" origin. The $556\ cm^{-1}$, $693\ cm^{-1}$, $836\ cm^{-1}$ and $1071\ cm^{-1}$ features are assigned in a similar manner as E" vibronic states. The $210\ cm^{-1}$ band (see Fig.8) does not have an easily recognizable E" rotational contour (<u>vide infra</u>), but it may be assigned as E" with confidence, since its ν''_{16} hot band is polarized and an E" contour can be calculated for it. An A'_1 band is observed at $436\ cm^{-1}$ by its polarization behavior. No E' contours are identified.

It is somewhat more difficult to determine the vibrational parentage of each transition. The A'_1 band at $436\ cm^{-1}$ must be due to an e" vibration, since only e" x E" contains A'_1 in D_{3h}. It is thus either 16^1_0 (A'_1) or 10^1_0 (A'_1). Since it has a small isotope shift, 10^1_0 (A'_1), an out of plane hydrogen bending motion, can be ruled out. Also, the ν''_{16} hot band of this transition is unusually intense, implying that it is a sequence band (16^1_1). The weaker polarized feature at $445\ cm^{-1}$ in h_3 spectra is not a hot band and is tentatively assigned as 10_0^1 (A_2'). Since it does not evidence a 10_1^1 sequence band ca. -585 cm^{-1} and a comparable set of features is not located in d_3 spectra, this assignment remains less certain than 16_0^1 (A_1'). It should be noted that both these values (436 and 445 cm^{-1}) are quite different from those reported in Table II based on one photon results. However, both ν_{10} and ν_{16} are e" modes with vibronic components A_1' (two photon allowed), A_2' (forbidden), and E' (one photon allowed); thus the two experiments observe different vibronic components. In this work we have not analyzed the cause of this splitting but it must arise from either anharmonicities leading to ν_{16}-ν_{10} coupling, quadratic intrastate vibronic coupling, or strong Herzberg-Teller coupling with E', A_1', or A_2' electronic states. It would certainly be interesting to pursue the causes of these vibronic splittings.

The totally symmetric vibration 12_0^1(E") is identified by its known frequency[8], its similarity in line shape and structure to the origin, and by the non-totally symmetric modes built on it. Most of the remaining bands in the region below (0,0) + 1000 cm^{-1} are of E" vibronic symmetry and could be of a_1', a_2', or e' vibrational parentage. We rule out the a_1' totally symmetric vibrations since no Franck Condon progressions are observed and non-totally symmetric vibrations are not built on any of these features. Since isotope shifts are small for these low lying modes, ν_3', ν_{20}', and ν_9' may be eliminated as candidates. The ground state frequency of ν_{14} is too high and it can only appear via Herzberg-Teller coupling which would not be capable of producing the observed intensity. The only remaining vibrational assignments for the four E" bands below (0,0) + 1000 cm^{-1} are ν_8', ν_{19}', and ν_6'. Since in the one photon vibronically allowed spectrum, 6_0^1 (A_2'') has been assigned at 677 cm^{-1} we can assume that ν_6' is the lowest energy of the e' excited state modes; 8_0^1 (A_2'') and 19_0^1 (A_2'') appear to be over 1000 cm^{-1} (Table II) from the origin. Thus the two lowest E" bands (210 and 556 cm^{-1}) are assigned as components of ν_6' (6_0^1 (E") and 6_0^2 (E")), respectively. The unusual assignment of 6_0^1 (E") at 210 cm^{-1} is supported by the presence of a relatively intense sequence hot band 6_1^1 (E") at -476 cm^{-1}. From these arguments it is not obvious how the remaining two E" features below (0,0) + 1000 cm^{-1} should be labeled and we defer this discussion until Section VI.

Finally, the origin region will be discussed at greater length. An unusual feature appears at -24 cm^{-1}, as shown in Figure 5, which is not reproduced in rotational contour calculations of the E" origin. The most obvious assignment is 16_1^1 (E') but there are a number of observations which tend to contradict this assignment. The -24 cm^{-1} peak does not appear to increase enough in intensity upon heating to 100°C to be 16_1^1 (E'), but overlap with the origin contour and poor signal to noise ratio at 100°C make this result inconclusive. Moreover, such a feature is not observed to be associated with other E" contours (see Figures 5-8) and one would expect analogous sequence structure to appear on every feature of appropriate symmetry (i.e., 6_0^1 16_1^1 (E') and 6_0^2 16_1^1 (E')). It should be noted that 6_0^1 16_1^1 (A_1') and 6_0^2 16_1^1 (A_1') are observed. That such a feature is indeed missing on the other E" contours is confirmed by the fact that a ν_6'' hot band of the -24 cm^{-1} peak is easily observed, whereas no ν_6'' hot bands of the missing 6_0^1 16_1^1 (E') and 6_0^2 16_1^1 (E') can be seen. A feature analogous to the -24 cm^{-1} one does appear on the contour of the first totally symmetric built on the origin, 12_0^1 (E"). The ν_6'' hot band built on the -24 cm^{-1} feature is in fact more intense than 6_1^0 (E"), indicating that it might be of the sequence type, namely 6_1^1 (A_1''). This suggests that the -24 cm^{-1} feature could be related to the presence of ν_6' (A_1'') at the origin. How such a transition could obtain intensity is unclear, but since it is so near an intense feature, many perturbation mechanisms could be envisioned. Further discussion of this feature is postponed until JT calculations are discussed. J. Parkin has communicated to us that the one photon spectrum may also evidence an A_1'' feature "below the E" origin."

V. CALCULATIONS

A. $(E'' + A_2'') \times e'$ vibronic coupling.

General methods for vibronic coupling calculations may be found in references 21-23. A brief outline of the calculation is given here. We wish to emphasize that in spite of the differences between MF_6 and triazine, the overall methods and even the results are quite similar.

The two lowest excited states of sym-triazine are energetically close ($\sim$1500 cm^{-1}); thus vibronic coupling calculations should include not only vibronic coupling within the E'' manifold, but also between E'' and A_2'' manifolds. The Hamiltonian includes both LJT and QJT terms between E'' components but only linear terms between E'' and A_2'' components.

Since large matrices are diagonalized numerically, it is important to choose a basis set and phase convention which guarantees real matrix elements. Lax's convention seems most convenient for this purpose.[28] D_{3h} basis functions, matrix representations, and Clebsch-Gordon coefficients are then defined. A vibronic coupling matrix Hamiltonian appropriate for the $(E'' + A_2'')$ manifold is formed in the usual fashion utilizing the Wigner-Eckart theorem to reduce the number of independent parameters to the minimum determined by symmetry: D is the LJT parameter; $Q[a_1']$ and $Q[e']$ are the QJT parameters; D' is the LPJT parameter which gauges the vibronic interaction between the E'' and A_2'' manifolds, and ΔE is their separation. Next, a symmetry-adapted vibronic basis is formed. The first step is to determine appropriate combinations of two-dimensional harmonic oscillator functions of the usual polar coordinate type which transform according to the irreducible representations of D_{3h}. These may then be combined with electronic factors using Clebsch-Gordon coefficients. Secular energy matrices are formed by taking matrix elements of the symmetry adapted basis functions with the matrix Hamiltonian. Separate E", A''_2, A''_1 blocks are thereby formed. General formulae for the matrix elements of harmonic oscillator function with powers of vibrational coordinates are available.[29] We have used a basis formed from all appropriate harmonic oscillator functions up to $n = 20$. Details of this calculation are given in the appendix.

Examples of these calculations are given in Figures 10 and 11 and Table V. In Figure 10, the effect of LPJT coupling is illustrated; in Figure 11 the regime of large QJT coupling with only a small LJT parameter is explored. These calculations will be compared with the experimental findings in Section VI. Table V provides precise numerical data which will allow comparison with other calculations.

B. Rotational Contour Calculations.

The rotational contour calculations were carried out in the usual manner.[19,30-32] Sym-triazine nuclear statistical weights were employed but seem to make little difference in the contours at the resolution used (0.5 cm^{-1}). The quantum number J was varied from 0 to 100. No line shape function was used for the individual transitions; all intensity was placed in a box covering 0.5 cm^{-1} and the points thus generated were connected with lines on a computer plotter.

VI. JAHN TELLER INTERPRETATION OF THE ν_6' MODE

The behavior of ν_6 in the E'' electronic state of sym-triazine is clearly highly unusual: large energy differences between 6^1_0 (A_2'') and 6^1_0 (E''); an anharmonic ν_6 progression; and many E'' modes within a 1000 cm^{-1} of the E'' origin. Reasons for this abnormal behavior are discussed in this section.

The electronic degeneracy of the E'' electronic state and the proximity of an A_2'' electronic ($\sim$1000 cm^{-1}) state strongly suggest that some form of vibronic interaction (JT or PJT) is responsible for the highly irregular nature of ν_6' bands.

It is immediately clear upon examining Figure 10 that PJT interaction between E'' and A_2'' electronic states is not responsible for the observed ν_6' behavior since it places the E'' ν_6 vibronic components <u>above</u> the A_2'' ν_6 components. Experimentally, the lowest E'' ν_6' is observed at 210 cm^{-1}, and one photon experiments place the A_2'' (6^1_0) at 677 cm^{-1}. Table VI shows that there is, however, a set of parameters for the JT calculation which qualitatively accounts for the observed ν_6' bands. In fact, the 693 cm^{-1} band which is not assigned in Section IV fits well as 6^3_0 (E'') and indeed is predicted to have considerable intensity. Based on these calculations, 6^4_0 is most likely assigned as the 836 cm^{-1} (E'') feature (see Table III for other possibilities, however). Strength of the $n\nu_6$ series interpretation is evidenced by the fact that six energy levels are approximately calculated with only two parameters (see Table VI). The calculation also reproduces the observations that A_2'' levels in the 0-1500 cm^{-1} region above the origin are sparse, and that there are many E'' levels in the 0-1500 cm^{-1} range. Moreover, an A_1'' comes into near coincidence with the origin, in agreement with the perturbed origin contour.

The small coriolis coupling constant obtained from the rotational contour analysis of the E" origin (Section VB) supports the above interpretation since JT vibronic coupling is expected to quench electronic angular momentum. Further evidence for a substantial JT effect in the ν_6' progression is apparent from the variation of the moments of inertia for triazine in the $n\nu_6'$ vibronic states; these are respectively for n=0 to 3, .2126, .2172, .2126, and .2121.

Calculated intensity patterns for 6^1_n (A''_2) emission doe not agree well with the observed ones as reported in SVLF studies.[14,15] Inspection of the ν_6' (A''_2) 677 cm^{-1} eigenvector calculated with parameters D, D', Q[e'], and ν° given in Table VI, shows I (6^1_3) larger than observed relative to I (6^1_2) and I (6^2_4). The proximity of 6^1_0 (A''_2) at 677 cm^{-1} and 6^3_0 (E") at 693 cm^{-1} may perturb the observed pattern, however. It is not unreasonable to expect only qualitative agreement here since several approximations have been made. Improvements might be realized by including cubic terms or simultaneous JT coupling with other e' vibrational modes (e.g., ν_8').[22] Certainly extensive Herzberg-Teller couplings are to be expected for this system and have been largely ignored in the calculation.

While substantial JT coupling in the E" electronic manifold is probably to be expected, it is however counter-intuitive that the QJT parameter Q[e'] is greater than the LJT parameter D. It may be that there is some "hidden" or approximate symmetry present in sym-triazine which tends to minimize LJT coupling. For example, many of the molecular orbitals of sym-triazine possess near cylindrical symmetry. Since ν_6' is an in-plane vibration, the entire electronic and vibrational coupling may mimic the cylindrical symmetry of a linear molecule; it is well known that LJT terms are zero for linear molecules (the Renner Teller Effect).

VII. CONCLUSIONS

Two photon photoacoustic spectra of the lowest excited state $^1E''$ of sym-triazine have been obtained. The electronic symmetry has been shown to be E'' by direct observation of rotational contours of the origin band and by observation of hot bands associated with this origin. Electronic angular momentum of this state is quenched ($\zeta_e \sim 0.1$). ν_6' vibronic components dominate the remainder of the spectrum from 0-1500 cm^{-1} and possess highly irregular intervals. Large splittings exist between A_1'', A_2'', and E'' vibronic ν_6' components.

It has been possible to fit and explain such an unusual progression for ν_6' based on a vibronic coupling calculation which has QJT coupling terms Q[e'] larger by a factor of four than LJT coupling terms D. PJT coupling with the nearby A_2'' state appears not to be important for this energy level scheme.

The two photon photoacoustic experimental technique has been demonstrated to be a sensitive method for obtaining the data. It is complementary to fluorescence excitation detection techniques. Through the use of photoacoustic detection, interference of CN photochemiluminescence was eliminated. The CN emission did, however, reproduce the photoacoustic spectrum in all essential features.

ACKNOWLEDGEMENT

We would like to thank Dr. J. Parkin for giving us a copy of J. Barnard's thesis, and for helpful discussions about sym-triazine over the years.

REFERENCES

1. C. Grundmann, A. Kreutzberger, J. Am. Chem. Soc. 76, 632 (1954).
2. R. C. Hirt, F. Halverson, R. G. Schmitt, J. Chem. Phys. 22, 1148 (1954).
3. J. E. Lancaster, N. B. Colthup, J. Chem. Phys. 22, 1149 (1954).
4. J. S. Brinen, L. Goodman, J. Chem. Phys. 31, 482 (1959); 35, 1219 (1961).
5. J. E. Lancaster, R. F. Stamm, N. B. Colthup, Spectrochem. Acta 17, 155 (1961).
6. K. K. Innes, J. P. Byrne, I. G. Ross, J. Mol. Spec. 22, 125 (1967).
7. Y. Udagawa, M. Ito, S. Nagakura, J. Mol. Spec. 39, 400 (1971).
8. G. Fischer, G. J. Small, J. Chem. Phys. 56, 5934 (1972).
9. R. M. Hochstrasser, A. H. Zewail, Chem. Phys. Lett. 11, 157 (1971); J. Chem. Phys. 55, 5291 (1971).
10. R. M. Hochstrasser, Chem. Phys. Lett. 17, 1 (1972).
11. R. M. Hochstrasser, T. S. Lin, A. H. Zewail, J. Chem. Phys. 56, 637 (1972).
12. T. J. Aartsma, D. A. Wiersma, Chem. Phys. 1, 211 (1973).
13. E. R. Bernstein, R. E. Smalley, J. Chem. Phys. 58, 2197 (1973); Chem. Phys. 2, 321 (1973).
14. A. E. W. Knight, C. S. Parmenter, Chem. Phys. 43, 257 (1979).
15. A. E. W. Knight, C. S. Parmenter, Chem. Phys. 15, 85 (1976).
16. P. R. Nott, B. K. Selinger, Aust. J. Chem. 31, 1889 (1978).
17. J. D. Webb, K. M. Swift, E. R. Bernstein, J. Mol. Structure 61, 285 (1980).
18. J. H. Callomon, T. M. Dunn, I. M. Mills, Philos. Trans. R. Soc. London Ser. A.259, 499 (1965).
19. F. Metz, W. E. Howard, L. Wunsch, H. J. Neusser, E. W. Schlag, Proc. Roy. Soc. London A363, 381 (1978).

20. J. van Egmond, J. H. van der Waals, Mol. Phys. 28, 457 (1974).

21. G. R. Meredith, J. D. Webb, E. R. Bernstein, Mol. Phys. 34, 995 (1977).

22. E. R. Bernstein, J. D. Webb, Mol. Phys. 37, 191 (1979).

23. E. R. Bernstein, J. D. Webb, Mol. Phys. 36, 1113 (1978).

24. J. Barnard, Ph.D. Thesis, University College, London (1974).

25. R. E. Smalley, Ph.D. Thesis, Princeton University (1973).

26. J. J. Barrett, Private Communication.

27. K. M. Chen, E. S. Yeung, J. Chem. Phys. 69, 43 (1978).

28. M. Lax, Symmetry Principles in Solid State and Molecular Physics, Wiley-Interscience, New York (1974).

29. C. DiLauro, J. Mol. Spec. 41, 598 (1972).

30. W. Martin McClain, Robert A. Harris, Excited States, Volume 3, Ed. E.C. Lim, Academic Press, NY (1977), p. 1-56.

31. L. Wunsch, F. Metz, H. J. Nuesser, E. W. Schlag, J. Chem. Phys. 66, 386 (1977).

32. J. R. Lombardi, R. Wallenstein, T. W. Hänsch, D. M. Friedrich, J. Chem. Phys. 65, 2357 (1976).

TABLE 1. Ground state vibrations of sym-triazine.

Symmetry Type	Predominant Motion of Mode	Lord Numbering[(a)]	Frequency (cm^{-1})[(b)] h_3	d_3
a_1'	Hydrogen stretch	2	3042	2293
	In-plane ring bend	12	1132	1077
	Ring stretch	1	992	987
a_2'	Ring stretch	14	1617	1586
	In-plane hydrogen bend	3 or 15	1251	951
e'	In-plane hydrogen bend	20	3056	2280
	Ring stretch	8	1556	1530
	Ring stretch	19	1410	1284
	In-plane hydrogen bend	9	1174	931
	In-plane ring bend	6	675	662
a_2''	Out-of-plane ring bend	5	925	861
	Out-of-plane ring bend	4	737	577
e''	Out-of-plane hydrogen bend	10	1031	846
	Out-of-plane ring bend	16	340	309

Ground State Rotational Constants (cm^{-1})[(c)]

$h_3 = .2146$ $d_3 = .19358$

---

a. R. C. Lord, A. L. Marston, F. A. Miller, Spectrochim. Acta 9, 113 (1957).

b. Reference 5.

c. J. E. Lancaster, B. P. Stoicheff, Can. J. Phys. 34, 1016 (1956).

TABLE 2. Electronic Origins and Vibrational Analysis of the $^1E''$ State Determined from One-Photon Spectra.

	Electronic Origin (cm^{-1})$^{(a)}$	Rotational Constant B' (cm^{-1})$^{(b)}$
h_3	30,870	0.212
d_3	30,989	0.191

	Vibration	h_3 (a)	d_3 (a)	h_3 (b)	d_3 (b)
e'	6	677($\parallel$)	664($\parallel$)	677	664
	2 x 6	--	--	1176	1145
	8	1176($\parallel$)	1145($\parallel$)	1005	960
	19	--	--	1105	1048
a_2''	4	359($\perp$)	278($\perp$)	359	278
	5	599(?)	559($\perp$)	599	559
e''	10	508($\perp$)	417($\perp$)	508	417
	16	303($\perp$)	273	308	280
a_1'	12	1081	1035	1081	1035

a. Reference 8.

b. Reference 24.

TABLE 3. Summary of observed two-photon spectra of sym-triazine (h_3) and (d_3).

λ_{vac}/Å h_3		$2\sigma_{vac}$/cm^{-1} h_3	$\Delta 2\sigma_{vac}$/cm^{-1} h_3	 d_3	I$^{(a)}$	Assignments$^{(b)}$
6634.0		30148	-729	-704	W	6^1_1 (A''_1)
6630.9		30162	-715	-692	W	
6628.2		30174	-703	-680	W	6^0_1; 16^0_2
6624.5		30191	-686	-664	W	
6578.7		30401	-476	-465	W	6^1_1 (E'')
6550.8		30531	-346	-313	W	$16^0_1$$^{(c)}$
6528.3		30636	-241		W	$6^0_1\ 16^1_0$ (A'_1); $16^0_2\ 16^1_0$ (A'_1)
6506.2		30740	-137	-115	W	$16^0_1\ 6^1_0$ (E'')$^{(c)}$
6502.6		30757	-120		W	6^2_1 (E''); $16^0_2\ 6^2_0$ (E'')
6482.4		30852	- 24	- 28	W	6^1_0 (A''_1)(?); 16^1_1 (E')
6480.7		30861	- 16	- 16	S	Origin of E" electronic state (30869)
6477.3	h_3	30877$^{(d)}$	0		S	
	d_3	30995		0		
6474.3		30891	14	10	M	
6459.0		30965	88	96	W	
6455.3		30982	105	111	W	
6454.2		30988	111		W	16^1_1 (A'_1)
6436.2		31074	198	185	M	6^1_0 (E'') (31096)
6433.6		31087	210	201	S	
6432.6		31091	215	206	M	
6430.4		31102	225	218	M	

TABLE 3. (continued)

$\lambda_{vac}/\text{Å}$ h_3	$2\sigma_{vac}/cm^{-1}$ h_3	$\Delta 2\sigma_{vac}/cm^{-1}$ h_3	d_3	I$^{(a)}$	Assignments$^{(b)}$
6414.3	31180	303	297 314$^{(e)}$	M	$16^1_1\ 6^1_0$ (A_1')
6387.1	31313	436	413	M	16^1_0 (A_1')$^{(c)}$
6385.3	31322	445		M	10^1_0 (A_1')$^{(c)}$ (?)
6375.1	31372	495	476	W	$16^0_1\ 6^4_0$ (E'') $\left[16^0_1\ 8^1_0 \text{ (E'') or } 16^0_1\ 19^1_0 \text{ (E'')}\right]^{(c)}$
6366.1	31416	539	535	S	
6362.8	31433	556	548	VS	6^2_0 (E'') (31425)
6360.0	31446	570	562	M	
6343.7	31527	650		W	$16^1_1\ 6^2_0$ (A_1')
6340.7	31542	665		W	
6338.2	31555	678	665	M	6^3_0 (E'') (31562)
6335.0	31570	693	675 680$^{(e)}$	M	
6332.1	31585	708	692	M	
6328.5	31603	726		W	
6309.0	31701	824	771	M	6^4_0 (E'') $\left[8^1_0 \text{ (E'') or } 19^1_0 \text{ (E'')}\right]$ (31705)
6306.5	31713	836	791	S	
6303.0	31731	854	799 804$^{(e)}$	M	
6288.9	31802	925		W	
6270.4	31896	1019		W	
6267.1	31912	1036	996	VS	$12^1_0\ 6^1_0$ (A_1'')
6263.1	31933	1056	1009	VS	12^1_0 (E'') (31940)
6260.3	31948	1071	1020	VS	
6238.2	32061	1184		S	
6227.5	32116	1239		M	
6224.4	32131	1254		M	
6218.8	32160	1283	1224 1240$^{(e)}$	M	$12^1_0\ 6^1_0$ (E'')

TABLE 3. (Continued)

$\lambda_{vac}/Å$ h_3	$2\sigma_{vac}/cm^{-1}$ h_3	$\Delta 2\sigma_{vac}/cm^{-1}$ h_3	d_3	I (a)	Assignments (b)
6207.8	32218	1340		S	
6203.9	32237	1360		S	
6199.3	32261	1385		S	
6175.8	32384	1507	1430	M	$12^1_0\ 16^1_0$ (A_1')
6156.5	32486	1609		S	
6153.3	32503	1626	1568	VS	$12^1_0\ 6^2_0$ (E")
6149.8	32521	1644		S	
6148.1	32530	1653		S	
6141.4	32566	1689		M	
6128.8	32633	1756		S	
6120.7	32676	1799		VS	
6101.1	32781	1904		M	$12^1_0\ 6^4_0$ (E") $\left[12^1_0\ 8^1_0\right.$ (E") or $12^1_0\ 19^1_0$(E")]
6064.1	32981	2104		VS	
6055.0	33031	2154		M	
6051.5	33050	2173		M	
6034.6	33142	2265		M	
6030.3	33166	2289		M	

---

a. I = Intensity; W = Weak; M = Moderate; S = Strong; VS = Very Strong.

b. See text (Section IV) for explanations. Parenthetical symmetry is excited state symmetry. Rotationless origins are given in parentheses (± 3 cm^{-1}) for h_3-sym-triazine.

c. Feature shows change in intensity with circularly polarized light.

d. This strong, sharp feature is taken as the origin for purposes of measuring $\Delta 2\sigma_{vac}$ and approximate vibrational intervals.

e. Features in d_3 are split.

TABLE 4. Vibronic Symmetries and Selection Rules in an E" State.

D_{3h} Vibrational Symmetry	Vibronic Symmetry of First Quantum in E" Electronic State
a_1'	E''
a_2'	E''
e'	A_1'', A_2'', E''
a_2''	E'
e''	A_1', A_2', E'

Type	Vibronic Symmetry	Selection Rule
One-Photon	A_2''	$\Delta K = 0$ ∥
	E'	$\Delta K = \pm 1$ ⊥
Two-Photon	A_1'	$\Delta K = 0$ (a)
	E''	$\Delta K = \pm 1$
	E'	$\Delta K = \pm 2$

a. For $A_1' \leftarrow A_1'$ or $E'' \leftarrow E''$ the transition symmetry is A_1' ($\Delta K = 0$) and the isotropic part of the Q branch disappears if the transition is observed in circularly polarized light.

TABLE 5. Eigenvalue calculation for comparison purposes. (D is the LJT parameter, D' is the LPJT parameter, Q[a'] and Q[e'] are QJT parameters, ν_6' is the unperturbed frequency, and ΔE is the separation of $^1E''$ and $^1A_2''$.

---

20 Oscillators

D = 0.8 D' = 0.0 Q[a'] = 0.1 Q[e'] = 0.1 ν_6' = 670 cm^{-1}

E''	A_1''	A_2''
0.0	121.0730768	662.5011750
544.2449932	836.4067343	1335.080923
933.4890954	1594.795278	2030.169769
1217.029648	1853.831997	2289.965194
1452.966477	2370.623305	2781.397675
1761.027421	2685.216268	3171.999172
1880.895019	3036.137014	3306.544160
2229.304175	3336.987600	3707.878153

10 Oscillators

D = 0.1 D' = 0.1 Q[a'] = 0.1 Q[e'] = 0.1 ν_6' = 670 cm^{-1}

ΔE = 2000 cm^{-1}

0.0	381.8399697	710.7872126
709.6421346	1263.695364	1437.040730
1006.593879	1719.539355	2038.781471
1388.928001	2133.142081	2288.459417
1613.615720	2480.052105	2317.805388
1871.777141	3013.560704	2791.887116
2115.287101	3137.603136	3080.915056

TABLE 6. Calculated best fit for ν_6 energy levels in the $^1E''$ state.(a)

$\nu_6' = 650$ cm^{-1} D = 0.05 D' = 0.0 Q[a'] = 0.0 Q[e'] = 0.2

E''			A_1''		A_2''		
Calc.	Obs.	n=0 coeff.	Calc.	Obs.	Calc.	Obs.	n=1 coeff.
0	0	.625	46	-24 (?)	665	677	.144
301	227	-.634	445	--	1060	1176	-.355
576	556	-.138	889	--	1369	--	.750
685	693	-.348					
917	836(?)	.055					

---

a. Frequencies in cm^{-1}; rotationless spacings are given.

APPENDIX

Description of $(E'' + A_2'') \times e'$ Vibronic Coupling Calculation

A vibronic basis made up of electronic ($\psi_{-1}^{E''}$, $\psi_{+1}^{E''}$, $\psi^{A_2''}$) and two-dimensional harmonic oscillator functions ($\chi_{N,L}$) is generated, and symmetry types E", A_1'', and A_2'' are grouped together. E" basis functions of the (-1) type were used. For N = 0 to N = 20, L was run over its values N, N-2, ... 1 or 0. For a given (N,L), basis functions were generated from the following forms.

	E''
$L = 0$	$\chi_{N,0}\,\psi_{-1}^{E''}$
$MOD(L,3)=0;\ MOD(L,2)=0;\ L \neq 0$	$\sqrt{1/2}\,(\chi_{N,L}+\chi_{N,-L})\,\psi_{-1}^{E''}\ (E''\times a_1')$ AND $\sqrt{1/2}\,(\chi_{N,L}-\chi_{N,-L})\,\psi_{-1}^{E''}(E''\times a_2')$
$MOD(L,3)=0;\ MOD(L,2)=1$	$\sqrt{1/2}\ i\,(\chi_{N,L}-\chi_{N,-L})\,\psi_{-1}^{E''}\ (E''\times a_1')$ AND $\sqrt{1/2}\ i\,(\chi_{N,L}+\chi_{N,-L})\,\psi_{-1}^{E''}(E''\times a_2')$
$MOD(L,3)=1;\ MOD(L,2)=0$	$\chi_{N,L}\,\psi_{+1}^{E''}$ AND $\chi_{N,-L}\,\psi^{A_2''}$
$MOD(L,3)=1;\ MOD(L,2)=1$	$-i\,\chi_{N,L}\,\psi_{+1}^{E''}$ AND $i\,\chi_{N,-L}\,\psi^{A_2''}$
$MOD(L,3)=2;\ MOD(L,2)=0$	$\chi_{N,-L}\,\psi_{+1}^{E''}$ AND $\chi_{N,L}\,\psi^{A_2''}$
$MOD(L,3)=2;\ MOD(L,2)=1$	$-i\,\chi_{N,-L}\,\psi_{+1}^{E''}$ AND $i\,\chi_{N,L}\,\psi^{A_2''}$

A_1''

MOD (L,3) = 1 ; MOD (L,2) = 0	$\sqrt{1/2}\,(\chi_{N,L}\,\psi_{-1}^{E''} + \chi_{N,-L}\,\psi_{+1}^{E''})$
MOD (L,3) = 1 ; MOD (L,2) = 1	$\sqrt{1/2}\; i\,(-\chi_{N,L}\,\psi_{-1}^{E''} + \chi_{N,-L}\,\psi_{+1}^{E''})$
MOD (L,3) = 2 ; MOD (L,2) = 0	$\sqrt{1/2}\,(\chi_{N,-L}\,\psi_{-1}^{E''} + \chi_{N,L}\,\psi_{+1}^{E''})$
MOD (L,3) = 2 ; MOD (L,2) = 1	$\sqrt{1/2}\; i\,(-\chi_{N,-L}\,\psi_{-1}^{E''} + \chi_{N,L}\,\psi_{+1}^{E''})$
MOD (L,3) = 0; MOD (L,2) = 0; L ≠ 0	$\sqrt{1/2}\,(\chi_{N,L} - \chi_{N,-L})\,\psi^{A_2''}$
MOD (L,3) = 0; MOD (L,2) = 1	$\sqrt{1/2}\; i\,(\chi_{N,L} + \chi_{N,-L})\,\psi^{A_2''}$

A_2''

MOD(L,3) = 1 ; MOD(L,2) = 0	$\sqrt{1/2}\,(\chi_{N,L}\,\psi_{-1}^{E''} - \chi_{N,-L}\,\psi_{+1}^{E''})$
MOD(L,3) = 1 ; MOD(L,2) = 1	$-\sqrt{1/2}\; i\,(\chi_{N,L}\,\psi_{-1}^{E''} + \chi_{N,-L}\,\psi_{+1}^{E''})$
MOD(L,3) = 2 ; MOD(L,2) = 0	$\sqrt{1/2}\,(\chi_{N,-L}\,\psi_{-1}^{E''} - \chi_{N,L}\,\psi_{+1}^{E''})$
MOD(L,3) = 2 ; MOD(L,2) = 1	$-\sqrt{1/2}\; i\,(\chi_{N,-L}\,\psi_{-1}^{E''} + \chi_{N,L}\,\psi_{+1}^{E''})$
L = 0	$\chi_{N,0}\,\psi^{A_2''}$
MOD(L,3) = 0 ; MOD(L,2) = 0 ; L ≠ 0	$\sqrt{1/2}\,(\chi_{N,L} + \chi_{N,-L})\,\psi^{A_2''}$
MOD(L,3) = 0 ; MOD(L,2) = 1	$\sqrt{1/2}\; i\,(\chi_{N,L} - \chi_{N,-L})\,\psi^{A_2''}$

The basis functions can be written in the general form

$$\Phi_{N,L} = (a\,\chi_{N,L} + b\,\chi_{N,-L})\,\psi_{-1}^{E''} + (c\,\chi_{N,L} + d\,\chi_{N,-L})\,\psi_{+1}^{E''} + (e\,\chi_{N,L} + f\,\chi_{N,-L})\,\psi^{A_2''}$$

Once the basis is generated, the matrix elements must be calculated. Only the upper (or lower) half of the matrix need be calculated, since the matrix is symmetric.

For linear JT coupling within the E" state we need the matrix Hamiltonian

$$\mathcal{H}_{LJT} = \begin{bmatrix} \mathcal{H}_0 & ikQ_- & 0 \\ -ikQ_+ & \mathcal{H}_0 & 0 \\ 0 & 0 & 0 \end{bmatrix}$$

and the primitive matrix elements

$$\langle \chi_{N,L} | Q_\pm | \chi_{N+1,L\mp1} \rangle = ((N \mp L + 2)/2\alpha)^{1/2} \qquad \alpha = \omega/\hbar$$

The LJT matrix elements can be worked out to

$$\langle \Phi_{N,L} | \mathcal{H}_{LJT} | \Phi_{N+1,L+1} \rangle = i\hbar\omega\,((N+L+2)D)^{1/2}\,(a^* c' - d^* b')$$

$$\langle \Phi_{N,L} | \mathcal{H}_{LJT} | \Phi_{N+1,L-1} \rangle = i\hbar\omega\,((N-L+2)D)^{1/2}\,(b^* d' - c^* a')$$

in which the primed coefficients are from the ket basis function, and $D = \frac{k^2}{2\hbar\omega^3}$

Similarly, the quadratic Hamiltonians are

$$\mathcal{H}^{a'}_{QJT} = \begin{bmatrix} \mathcal{H}_0 + \frac{C_a}{2} Q_+ Q_- & 0 & 0 \\ 0 & \mathcal{H}_0 + \frac{C_a}{2} Q_+ Q_- & 0 \\ 0 & 0 & 0 \end{bmatrix}$$

$$\mathcal{H}^{e'}_{QJT} = \begin{bmatrix} \mathcal{H}_0 & C_e Q_+^2 & 0 \\ C_e Q_-^2 & \mathcal{H}_0 & 0 \\ 0 & 0 & 0 \end{bmatrix}$$

The relevant primitive matrix elements are

$$\langle N,L | Q_\mp^2 | N,L\pm2 \rangle = \frac{1}{2\alpha}\left(4(N\mp L)(N\pm L+2)\right)^{1/2}$$

$$\langle N,L | Q_\mp^2 | N+2,L\pm2 \rangle = \frac{1}{2\alpha}\left((N\pm L+2)(N\pm L+4)\right)^{1/2}$$

$$\langle N,L | Q_+ Q_- | N,L \rangle = \frac{1}{2\alpha}(2N+2)$$

$$\langle N,L | Q_+ Q_- | N+2,L \rangle = \frac{1}{2\alpha}\left((N+L+2)(N-L+2)\right)^{1/2}$$

The quadratic JT diagonal matrix elements are then $(\langle E''\times a_1'' | \mathcal{H}^{a'}_{QJT} | E''\times a_2'' \rangle = 0)$

$$\langle \phi_{N,L} | \mathcal{H}^{a'}_{QJT} | \phi_{N,L} \rangle = \hbar\omega(1+Q[a']/2)(N+1) \qquad Q[a'] = \frac{C_a}{\omega^2}$$

$$\langle \phi_{N,1} | \mathcal{H}^{e'}_{QJT} | \phi_{N,1} \rangle = 2Q[e']\hbar\omega(N+1)(a^*d' + d^*a') \quad Q[e'] = \frac{C_e}{2\omega^2}$$

For diagonal in N, off diagonal in L we have

$$\langle \phi_{N,L} | \mathcal{H}^{e'}_{QJT} | \phi_{N,L+2} \rangle = 2Q[e']\hbar\omega\left((N-L)(N+L+2)\right)^{1/2}(b^*d' + c^*a')$$

$$\langle \phi_{N,L} | \mathcal{H}^{e'}_{QJT} | \phi_{N,L-2} \rangle = 2Q[e']\hbar\omega\left((N+L)(N-L+2)\right)^{1/2}(a^*c' + d^*b')$$

These two formulas must be corrected for L = 0 in either the bra or ket, since they do not account for the fact that since L = -L, a primitive matrix element that is usually zero is non-zero. For $\langle \phi_{N,0} | \mathcal{H}^{e'}_{QJT} | \phi_{N,2} \rangle$, $2Q[e']\hbar\omega(N(N+2))^{1/2}d'$ must be added to the above and for $\langle \phi_{N,2} | \mathcal{H}^{e'}_{QJT} | \phi_{N,0} \rangle$, $2Q[e']\hbar\omega(N(N+2))^{1/2}d^*$ must be added to the above. The quadratic matrix elements off diagonal in N and diagonal in L are

$$\langle \Phi_{N,L} | \mathcal{H}_{QJT}^{a'} | \Phi_{N+2,L} \rangle = \frac{\hbar\omega}{4} Q[a']((N+L+2)(N-L+2))^{1/2}(a^*a'+b^*b'+c^*c'+d^*d')$$

$$\langle \Phi_{N,1} | \mathcal{H}_{QJT}^{e'} | \Phi_{N+2,1} \rangle = \hbar\omega\, Q[e']((N+1)(N+3))^{1/2} \quad (a^*d'+d^*a')$$

The quadratic matrix elements off diagonal in N and L are

$$\langle \Phi_{N,L} | \mathcal{H}_{QJT}^{e'} | \Phi_{N+2,L+2} \rangle = \hbar\omega\, Q[e']((N+L+2)(N+L+4))^{1/2}(b^*d'+c^*a')$$

$$\langle \Phi_{N,L} | \mathcal{H}_{QJT}^{e'} | \Phi_{N+2,L-2} \rangle = \hbar\omega\, Q[e']((N-L+2)(N-L+4))^{1/2}(a^*c'+d^*b')$$

Again for L = 0 in the bra or ket we must correct the formulas. For $\langle \Phi_{N,0} | \mathcal{H}_{QJT}^{e'} | \Phi_{N+2,2} \rangle$ add $\hbar\omega Q[e']((N+2)(N+4))^{1/2} d'$, and for $\langle \Phi_{N,2} | \mathcal{H}_{QJT}^{e'} | \Phi_{N+2,0} \rangle$ add $\hbar\omega\, Q[e']((N+2)N)^{1/2} d^*$.

The matrix elements up to n = 10 were also hand calculated, and the hand calculation checked by the upper half of the matrix agreeing with the lower half.

The pseudo-Jahn Teller interaction between the E" and A_2'' was completed for basis functions to N = 10, and the matrix elements were hand calculated. The PJT matrix Hamiltonian is

$$\mathcal{H}_{PJT} = \begin{bmatrix} 0 & 0 & -ik'Q_+ \\ 0 & 0 & -ik'Q_- \\ ik'Q_- & ik'Q_+ & 0 \end{bmatrix}$$

We have derived the PJT matrix element formulas. They are as follows, with $D' = \frac{(k')^2}{2\hbar\omega^3}$:

$$\langle \phi_{N,L} | \mathcal{H}_{PJT} | \phi_{N+1,L+1} \rangle = -i\hbar\omega\left((N+L+2)D'\right)^{1/2}(b^*f' + c^*e')$$

$$\langle \phi_{N,L} | \mathcal{H}_{PJT} | \phi_{N+1,L-1} \rangle = -i\hbar\omega\left((N-L+2)D'\right)^{1/2}(a^*e' + d^*f')$$

$$\langle \phi_{N,L} | \mathcal{H}_{PJT} | \phi_{N-1,L+1} \rangle = -i\hbar\omega\left((N-L)D'\right)^{1/2}(b^*f' + c^*e')$$

$$\langle \phi_{N,L} | \mathcal{H}_{PJT} | \phi_{N-1,L-1} \rangle = -i\hbar\omega\left((N+L)D'\right)^{1/2}(a^*e' + d^*f')$$

We have the following additional factors:

for $\langle \phi_{N,0} | \mathcal{H}_{PJT} | \phi_{N+1,1} \rangle$ add $-i\hbar\omega\left((N+2)D'\right)^{1/2} f'$

for $\langle \phi_{N,1} | \mathcal{H}_{PJT} | \phi_{N+1,0} \rangle$ add $-i\hbar\omega\left((N+1)D'\right)^{1/2} d^*$

for $\langle \phi_{N,0} | \mathcal{H}_{PJT} | \phi_{N-1,1} \rangle$ add $-i\hbar\omega(ND')^{1/2} f'$

for $\langle \phi_{N,1} | \mathcal{H}_{PJT} | \phi_{N-1,0} \rangle$ add $-i\hbar\omega\left((N+1)D'\right)^{1/2} d^*$

FIGURE CAPTIONS

1a. Ground state n,π electronic structure.

1b. $\pi^* \leftarrow n$ spectroscopic transitions.

2. Role of vibronic coupling in single vibronic level fluorescence (SVLF). See text (Section II) for detailed discussion. The left hand side of the figure shows the electronic symmetry and the numbers indicate the number of quanta of ν_6. The right hand side shows the relevant vibronic symmetries of the levels. Double-ended arrows show vibronic coupling pathways. Single-ended arrows going down indicate possible emission. Solid lines are the LJT coupling case, dashed lines are the QJT coupling case.

3. Experimental two photon photoacoustic apparatus (see text for discussion).

4. Survey two photon photoacoustic spectrum of h_3-sym-triazine. Arrows indicate rotationless origins of labeled features. Horizontal axis is not linear in frequency, but in wavelength.

5a. Experimental rotational contour for d_3-sym-triazine $^1E''$ origin. Rotationless origin is marked with an arrow. Shoulder at low energy side of contour could be related to presence of 6_0^1 (A_1''). See text, Section IV for discussion.

5b. Calculated rotational contour of origin with $\Delta K = \pm 1$, $B'' = .19358$ cm^{-1}, $B' = .1916$ cm^{-1}, $C'' = B''/2$, $C' = B'/2$, $\zeta = +0.1$, $T = 298$ K. Frequency scale is same as for Figure 5a. Note missing shoulder on low energy side of contour.

6a. Experimental rotational contour for d_3-sym-triazine 6_0^2. Rotationless origin is marked with an arrow.

6b. Calculated rotational contour of 6_0^2 with $\Delta K = \pm1$, $B'' = .19358\ cm^{-1}$, $B' = .1916\ cm^{-1}$, $C'' = B''/2$, $C' = B'/2$, $\zeta = +0.1$, $T = 298\ K$. Frequency scale is same as for Figure 6a.

7a. Experimental rotational contour for d_3-sym-triazine 6_0^3. Rotationless origin is marked with an arrow.

7b. Calculated rotational contour of 6_0^3 with $\Delta K = \pm1$, $B'' = .19358\ cm^{-1}$, $B' = .1915\ cm^{-1}$, $C'' = B''/2$, $C' = B'/2$, $\zeta = 0.0$, $T = 298\ K$. Frequency scale is same as Figure 7a.

8a. Experimental rotational contour for d_3-sym-triazine 6_0^1. Rotationless origin is marked with an arrow.

8b. Calculated rotational contour of 6_0^1 with $\Delta K = \pm1$, $B'' = .19358\ cm^{-1}$, $B' = .1962\ cm^{-1}$, $C'' = B''/2$, $C' = B'/2$, $\zeta = -0.1$, $T = 298\ K$. Frequency scale is same as for Figure 8a.

8c. Experimental rotational contour for h_3-sym-triazine 6_0^1. Rotationless origin is marked with an arrow.

8d. Calculated rotational contour with $\Delta K = \pm1$, $B'' = .2146\ cm^{-1}$, $B' = .2172\ cm^{-1}$, $C'' = B''/2$, $C' = B'/2$, $\zeta = 0.0$, $T = 298\ K$. Frequency scale is same as for Figure 8c.

9. Experimental rotational contour for h_3-sym-triazine 16_0^1 (A_1') in both linear and circular polarization. Rotationless origin is marked with an arrow. The second polarized peak is a different transition, probably 10_0^1 (A_1').

10. Effect of LPJT parameter D' on first quantum of e' vibration in $^1E''$ electronic state. $\nu_6' = 670\ cm^{-1}$. D, Q[a'], Q[e'] are zero, ΔE, the separation of the E'' and A_2'' electronic states is $1500\ cm^{-1}$. Note that for this case, as well as for the LJT parameter D, the A_2'' level is <u>below</u> the E'' level, contrary to observation.

11. Effect of QJT parameter Q[e'] on ν_6 energy levels in $^1E''$ state with small LJT parameter D = 0.05, and D' = 0.0, Q[a'] = 0.0, $\nu_6' = 670$ cm^{-1}. Best fit (see Table VI) was found with Q[e'] = 0.2, but with $\nu_6' = 650$ cm^{-1}.

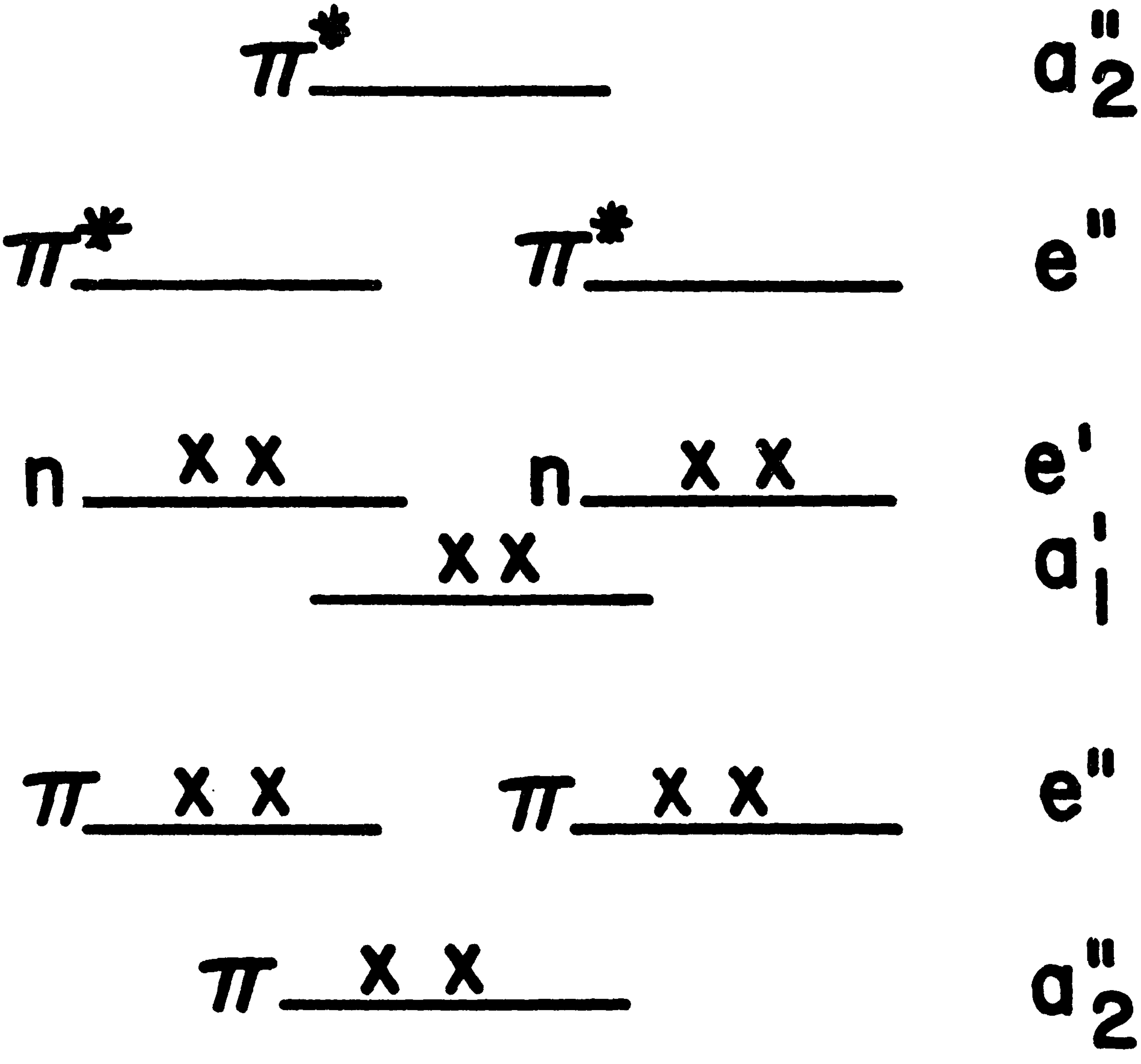

FIGURE 1a

ELECTRON PROMOTION	STATE SYMMETRY	TRANSITION TYPE
$\pi^*(e'') \leftarrow n(e')$	E''	2 PHOTON
	A''_2	1 PHOTON
	A''_1	———
$\pi^*(e'') \leftarrow n(a'_1)$	E''	2 PHOTON

FIGURE 1b

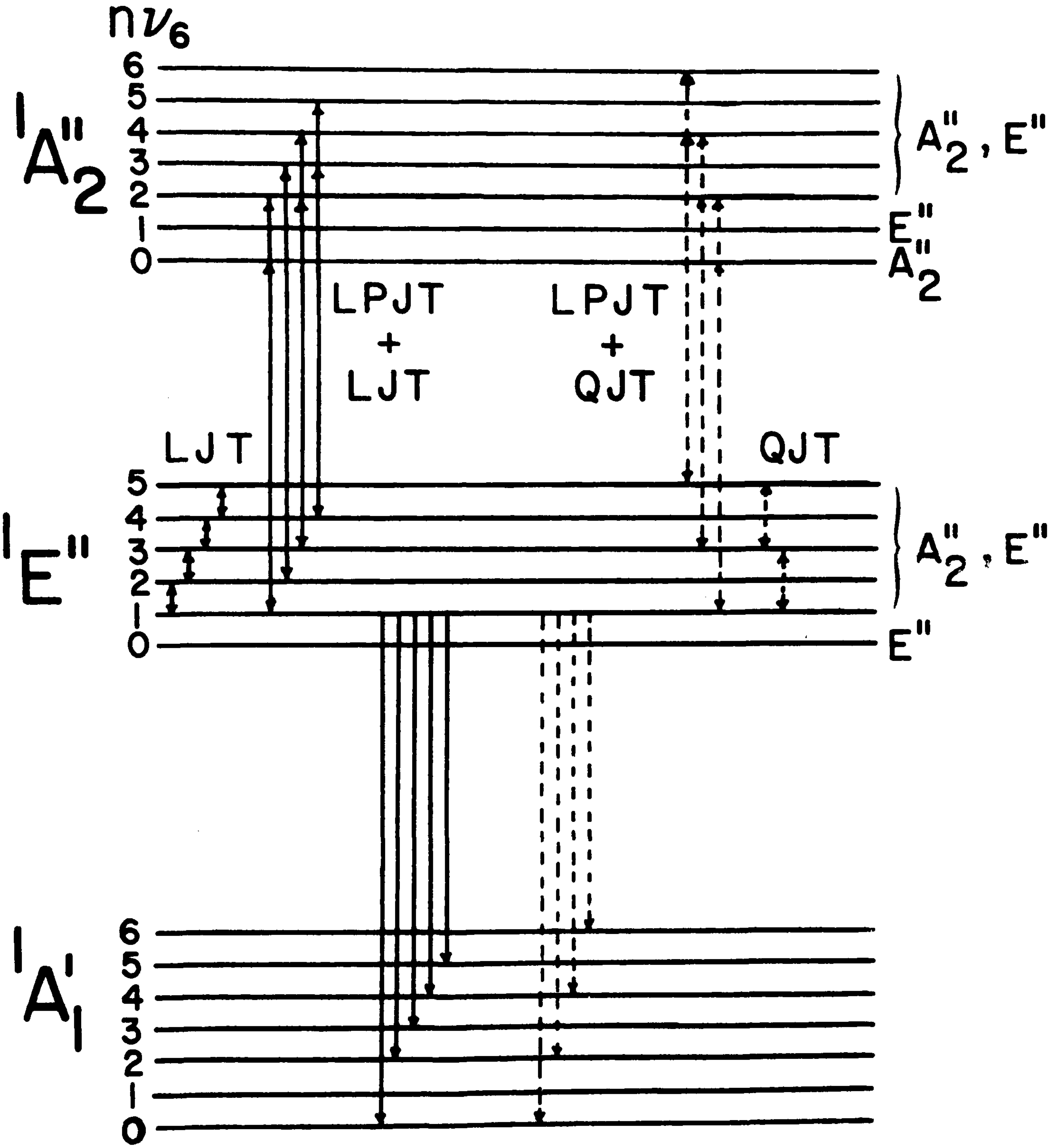

$n\nu_6$
$^1A_2''$
6
5
4
3
2
1
0
A_2'', E''
E''
A_2''
LPJT + LJT
LPJT + QJT
LJT
QJT
$^1E''$
5
4
3
2
1
0
A_2'', E''
E''
$^1A_1'$
6
5
4
3
2
1
0

FIGURE 2

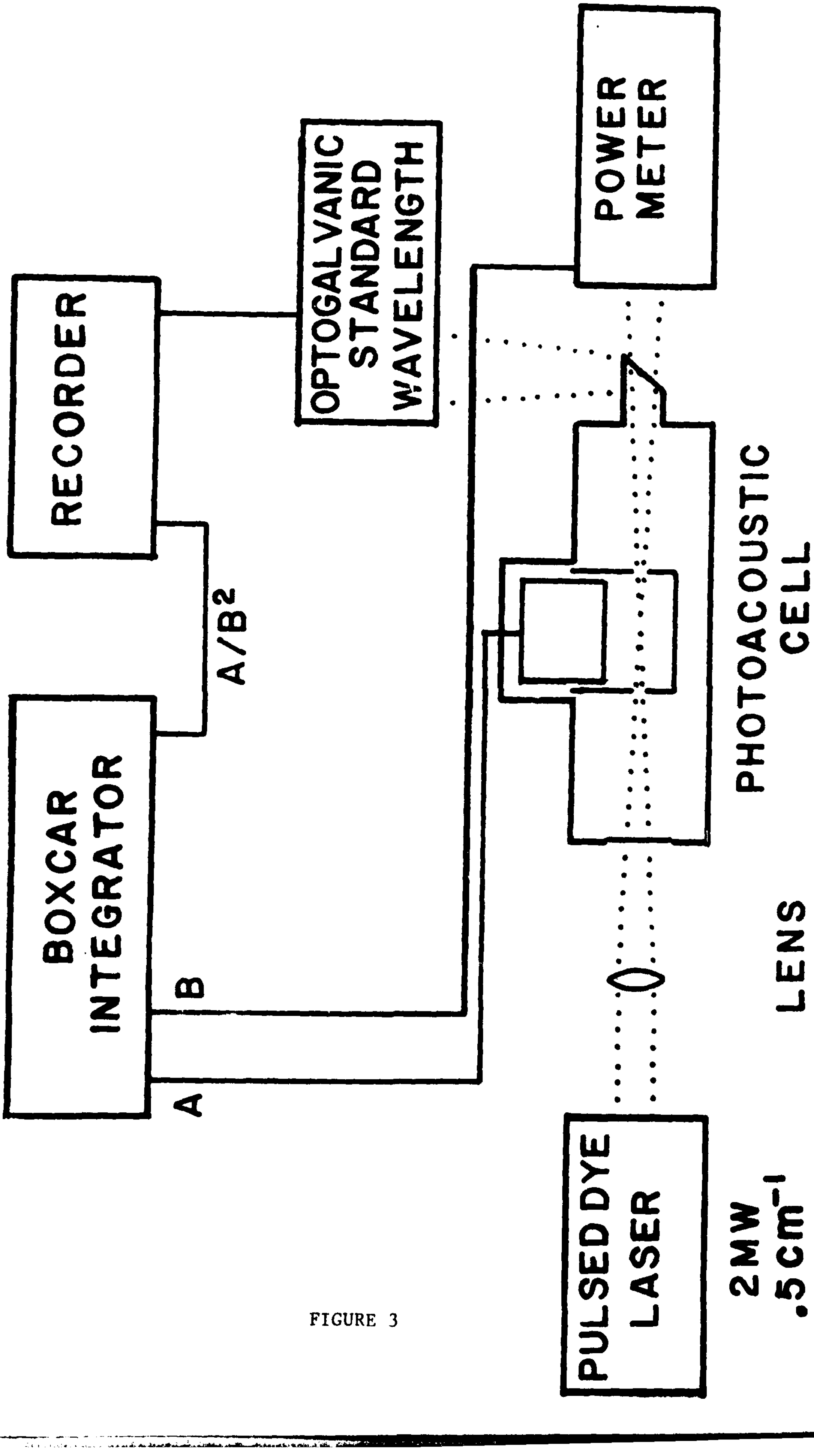
BOXCAR INTEGRATOR
A
B
A/B²
RECORDER
OPTOGALVANIC STANDARD WAVELENGTH
POWER METER
PHOTOACOUSTIC CELL
LENS
PULSED DYE LASER
2MW
.5cm⁻¹

FIGURE 3

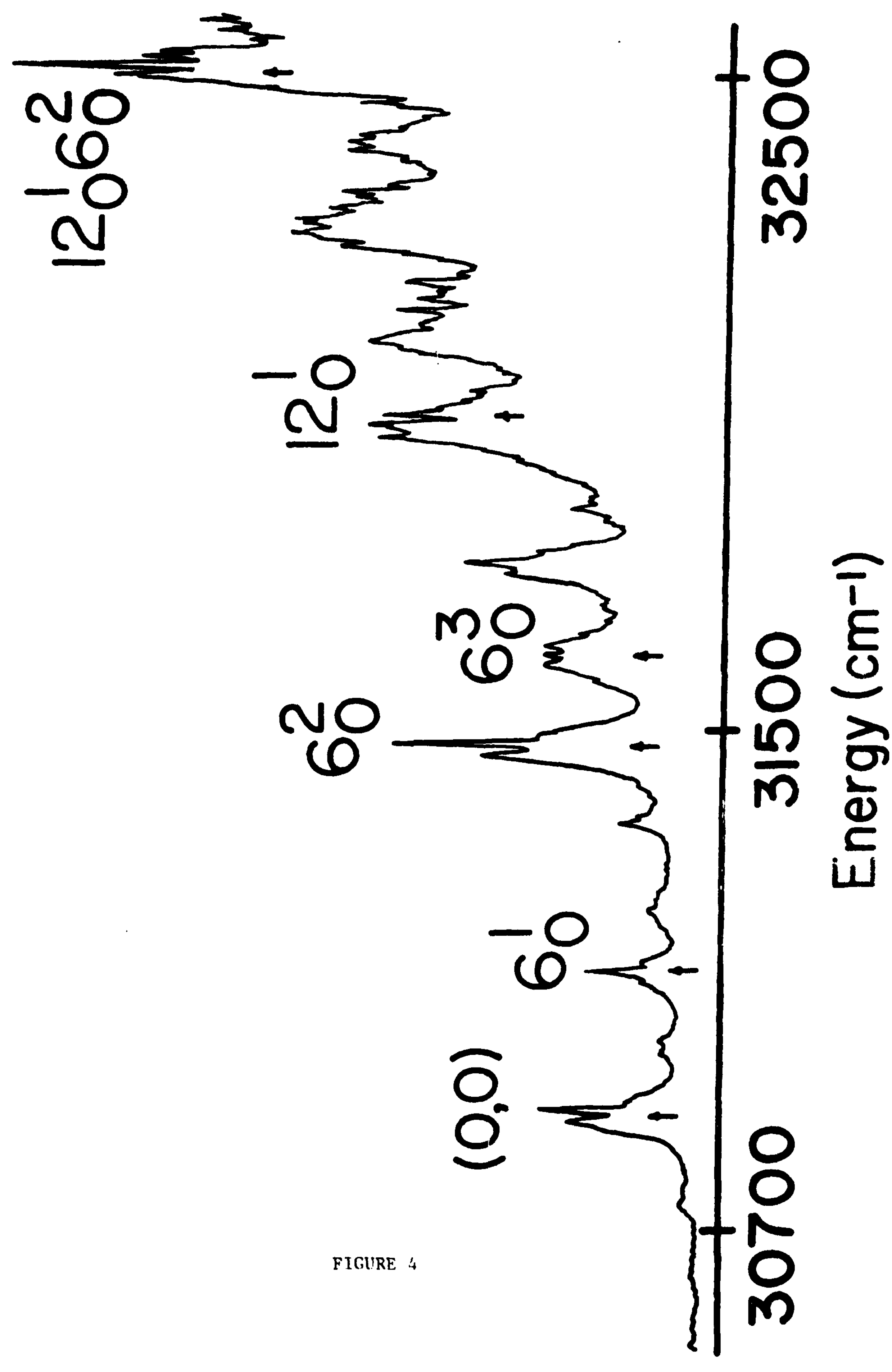

FIGURE 4

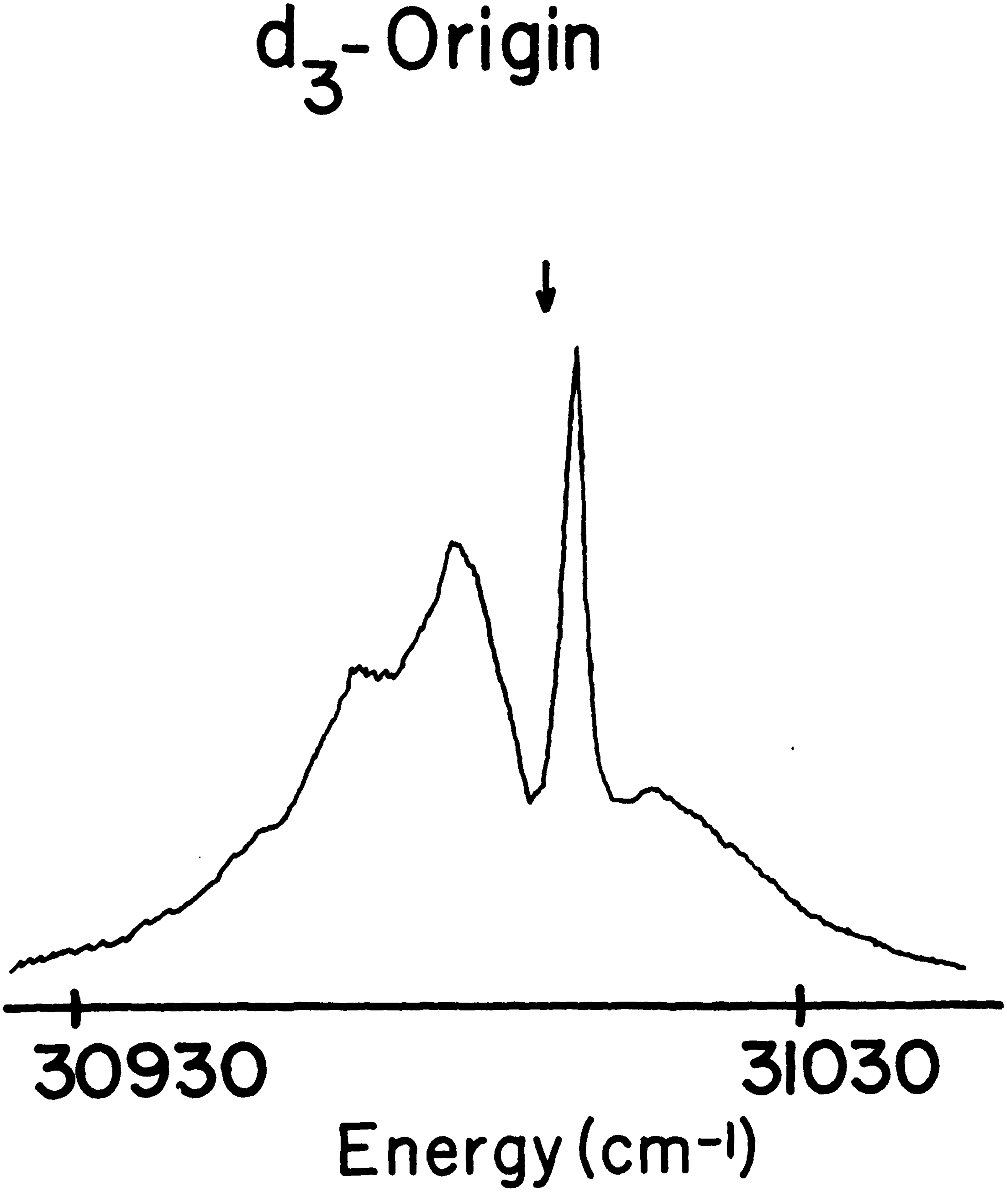

FIGURE 5a

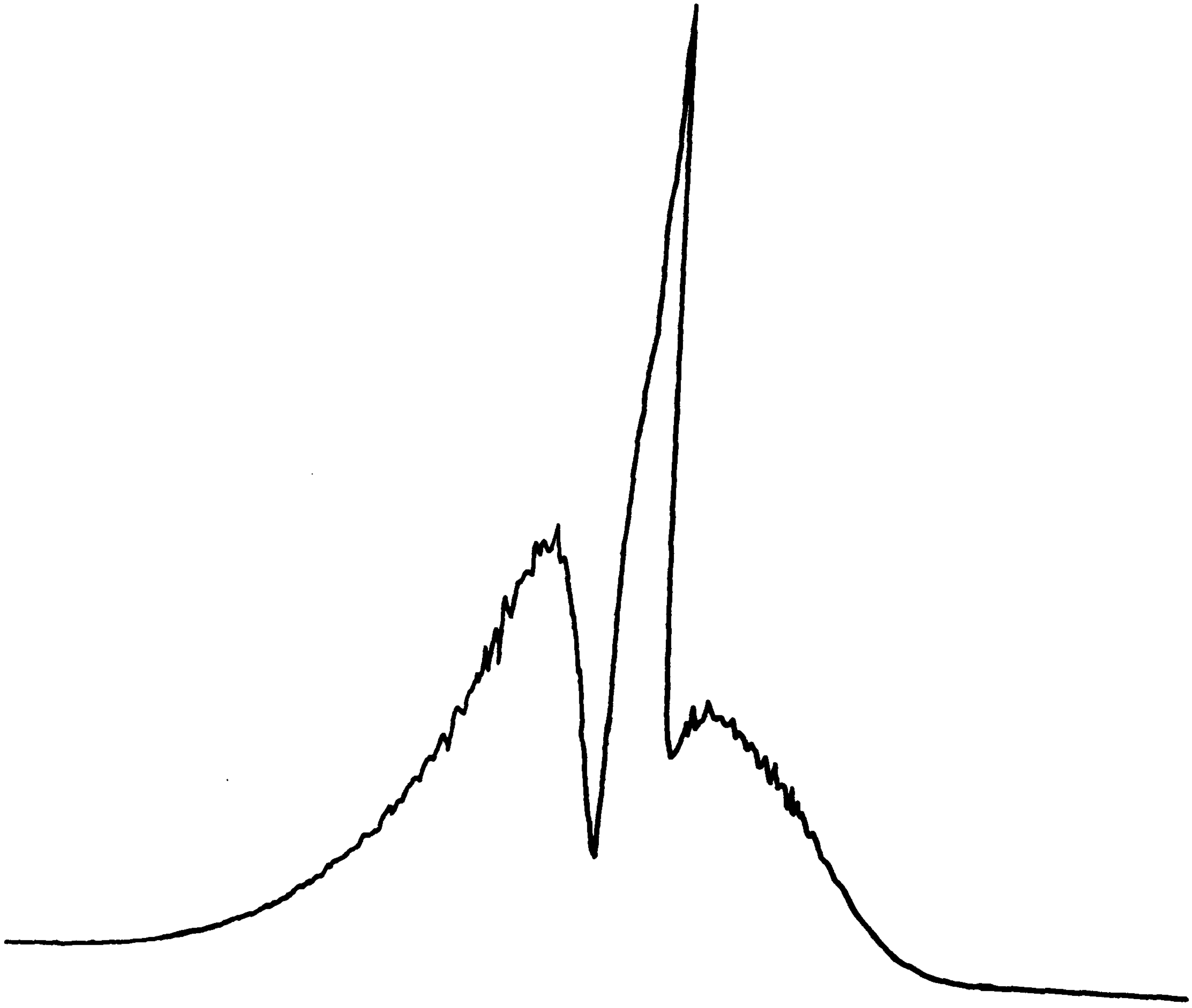

FIGURE 5b

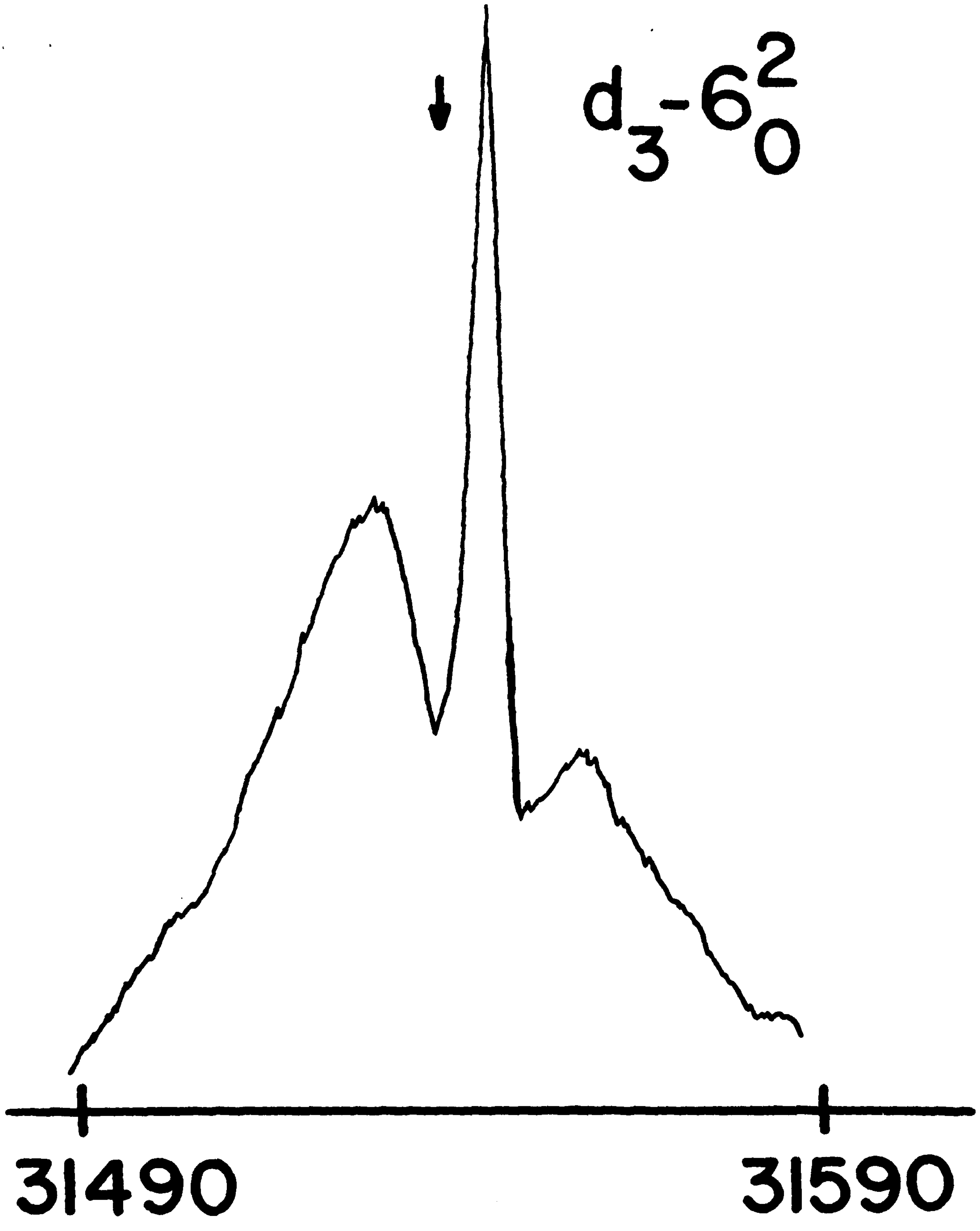

FIGURE 6a

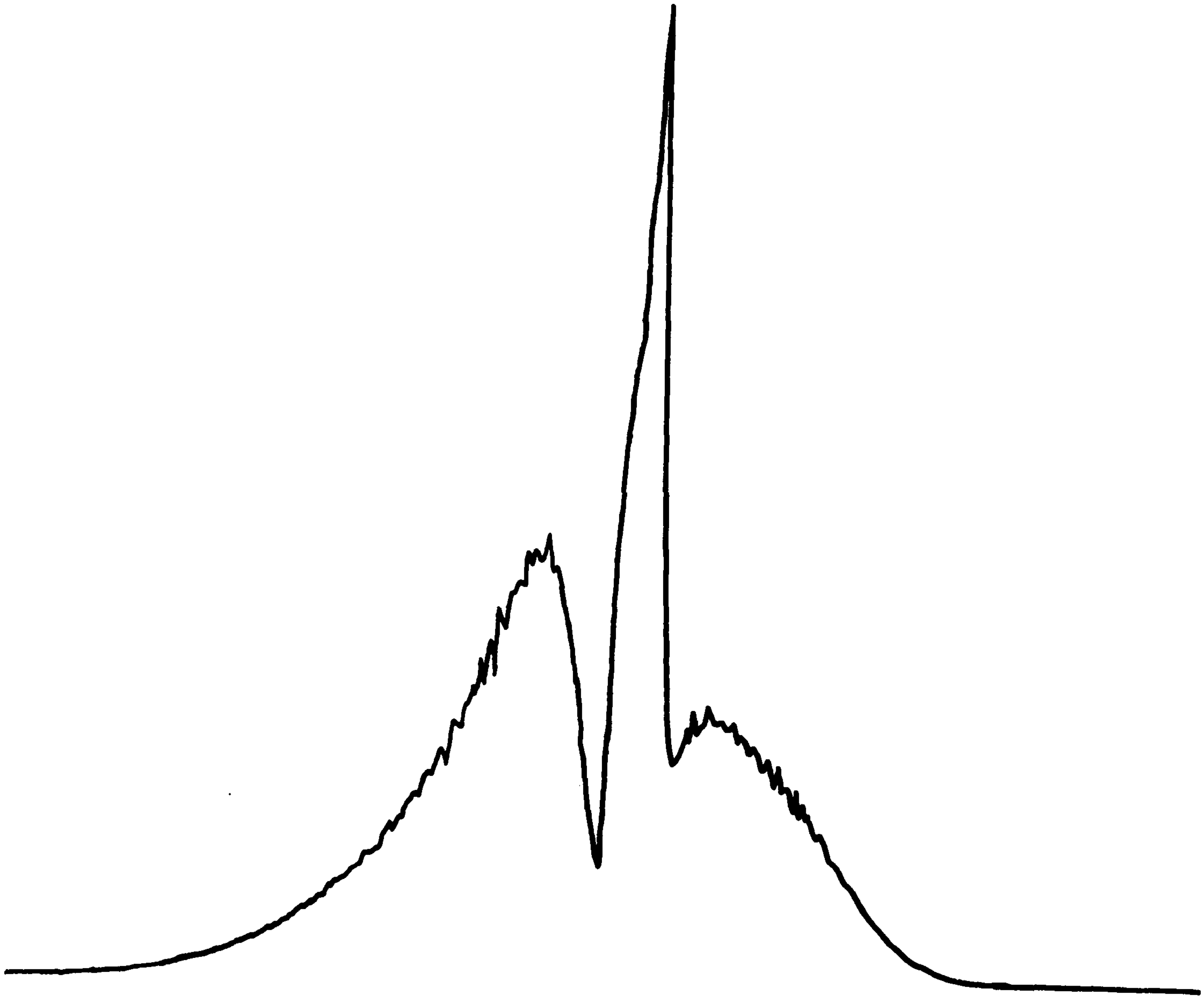

FIGURE 6b

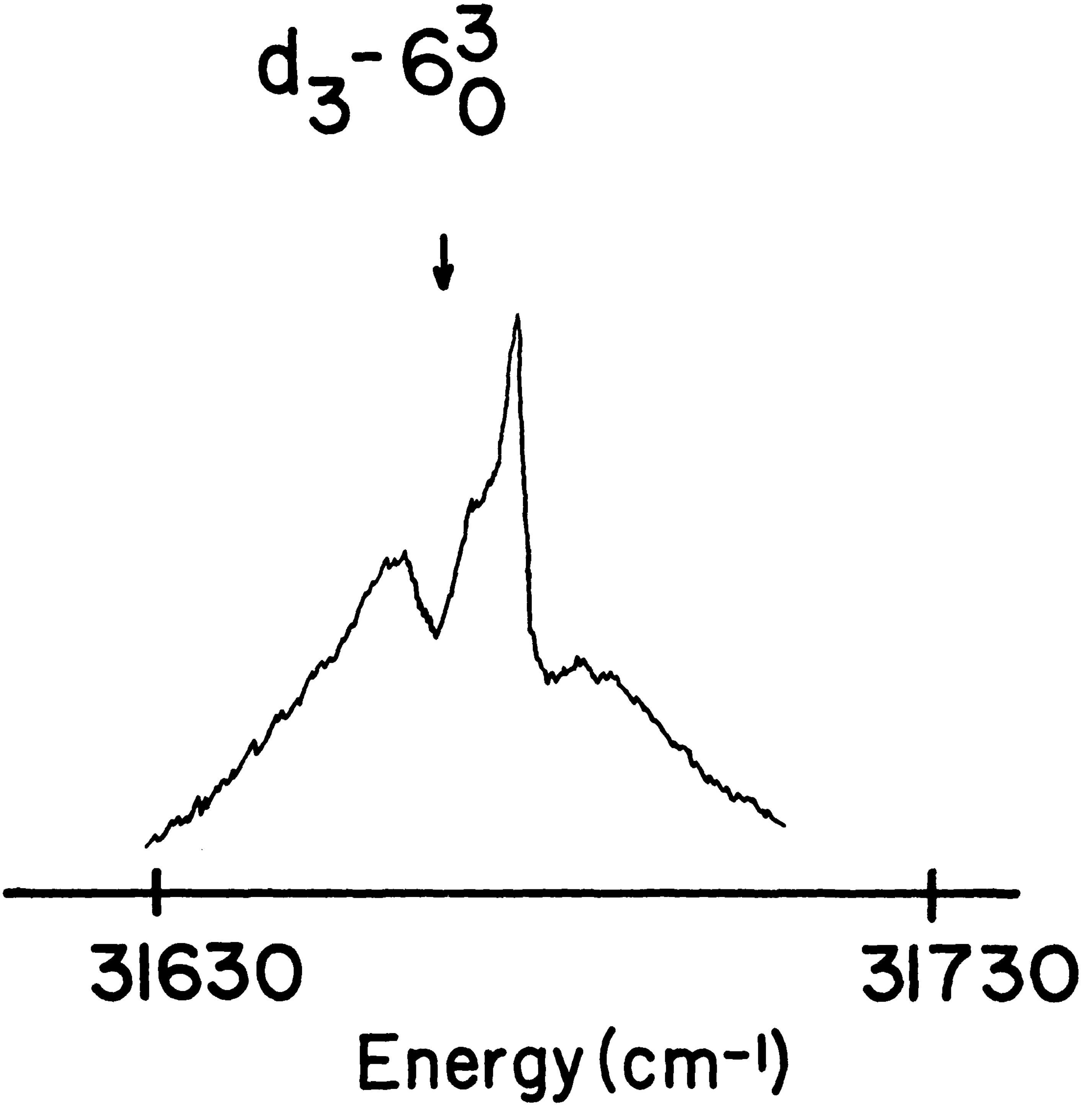

FIGURE 7a

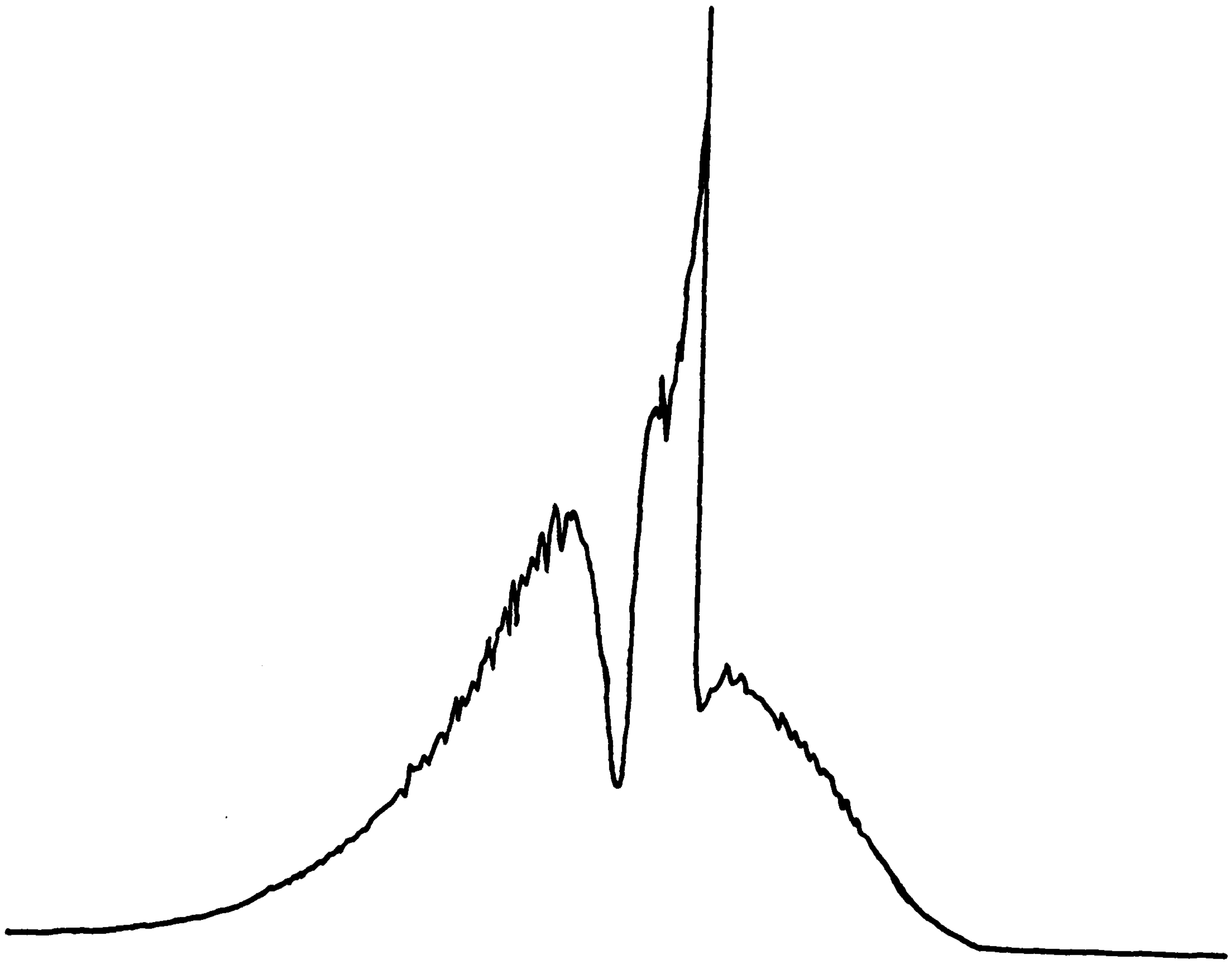

FIGURE 7b

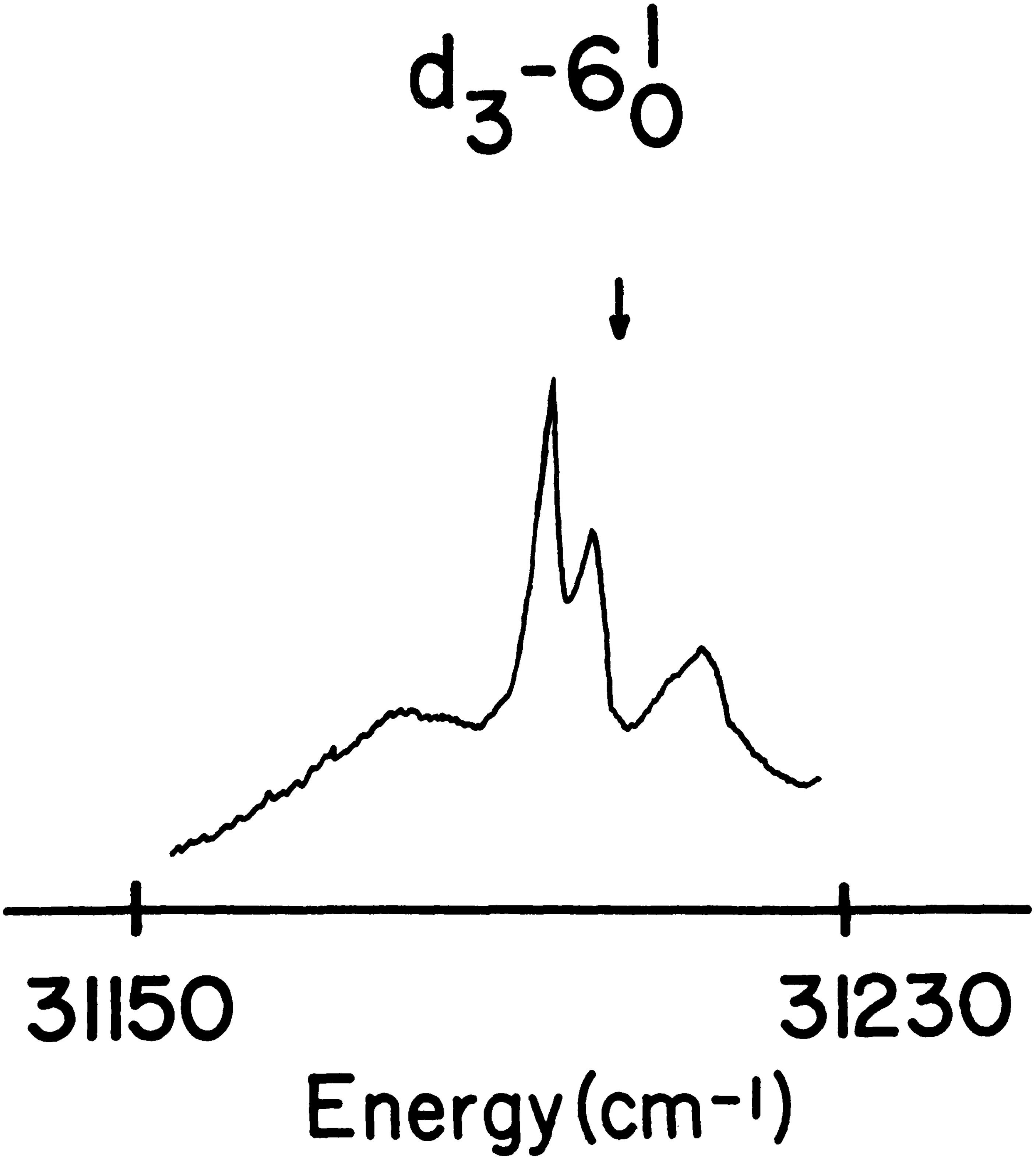

FIGURE 8a

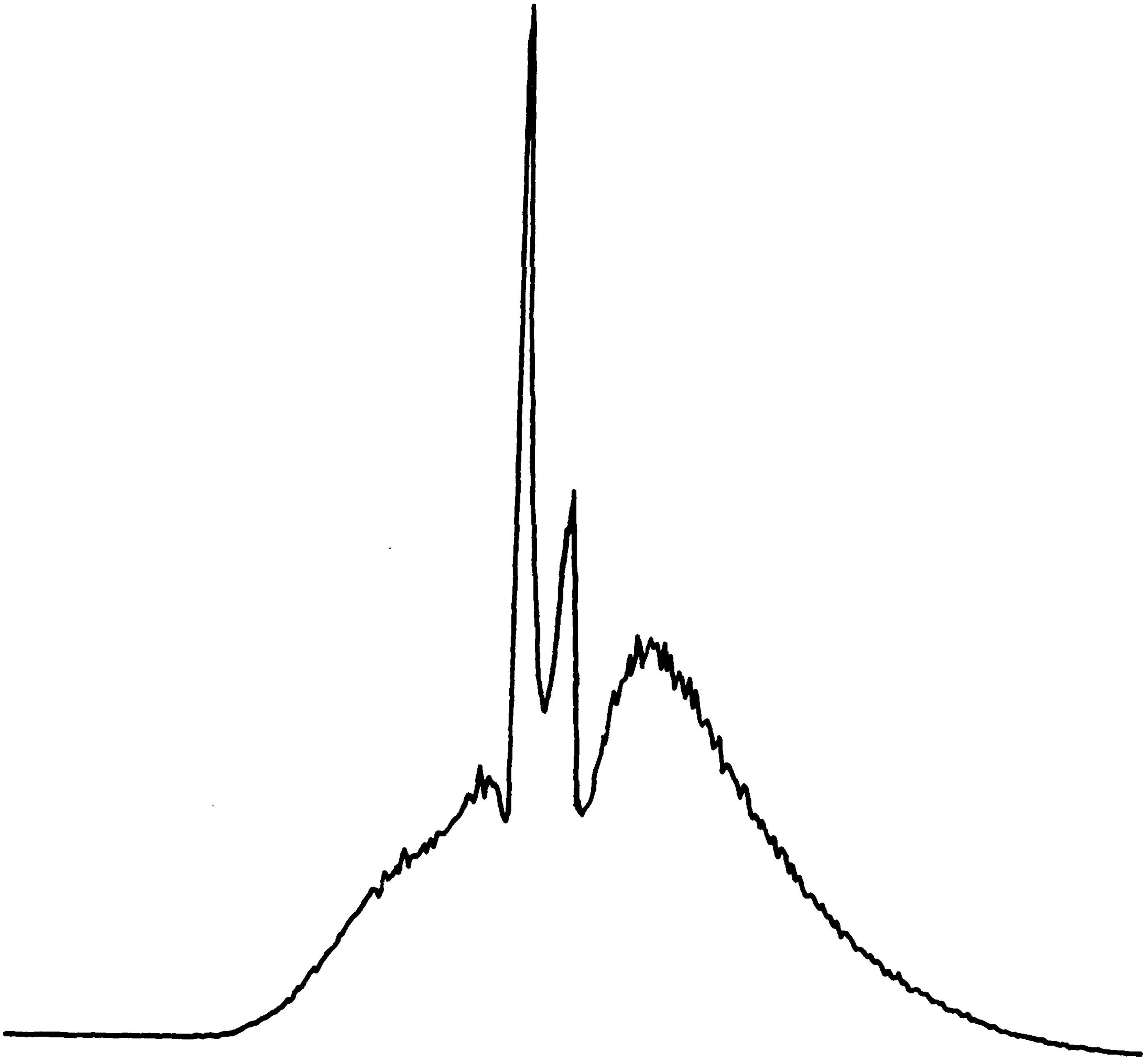

FIGURE 8b

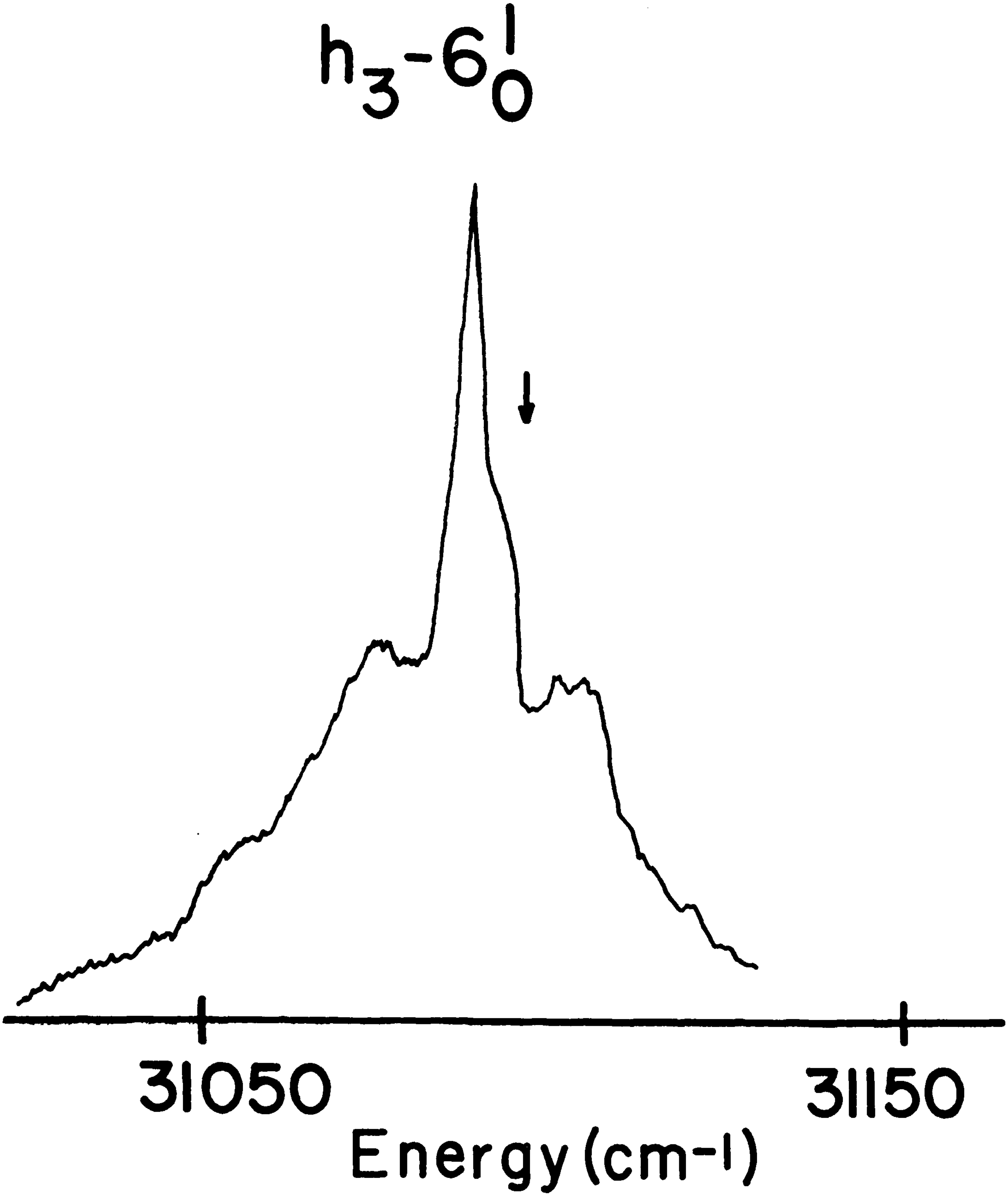

FIGURE 8c

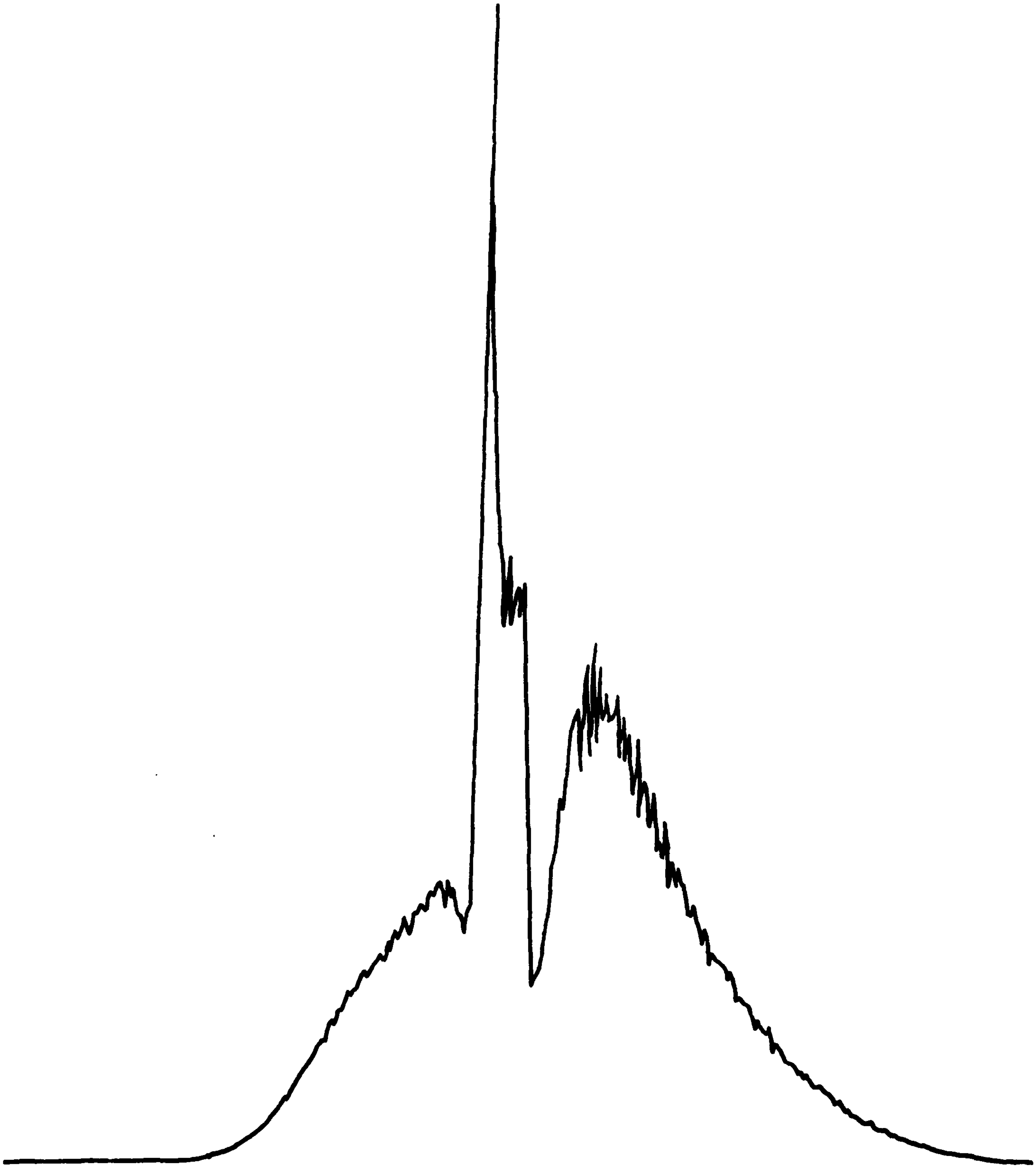

FIGURE 8d

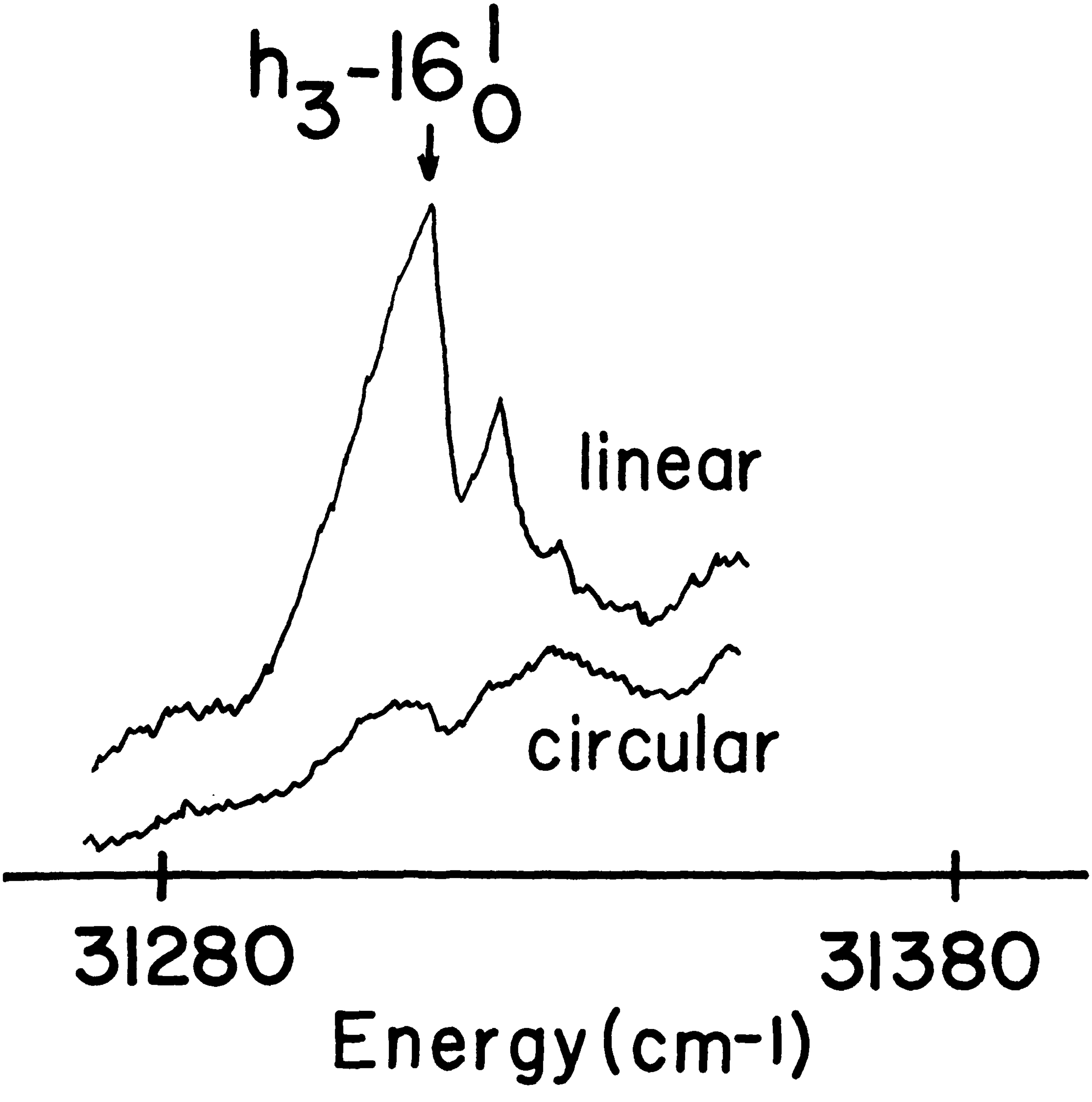

FIGURE 9

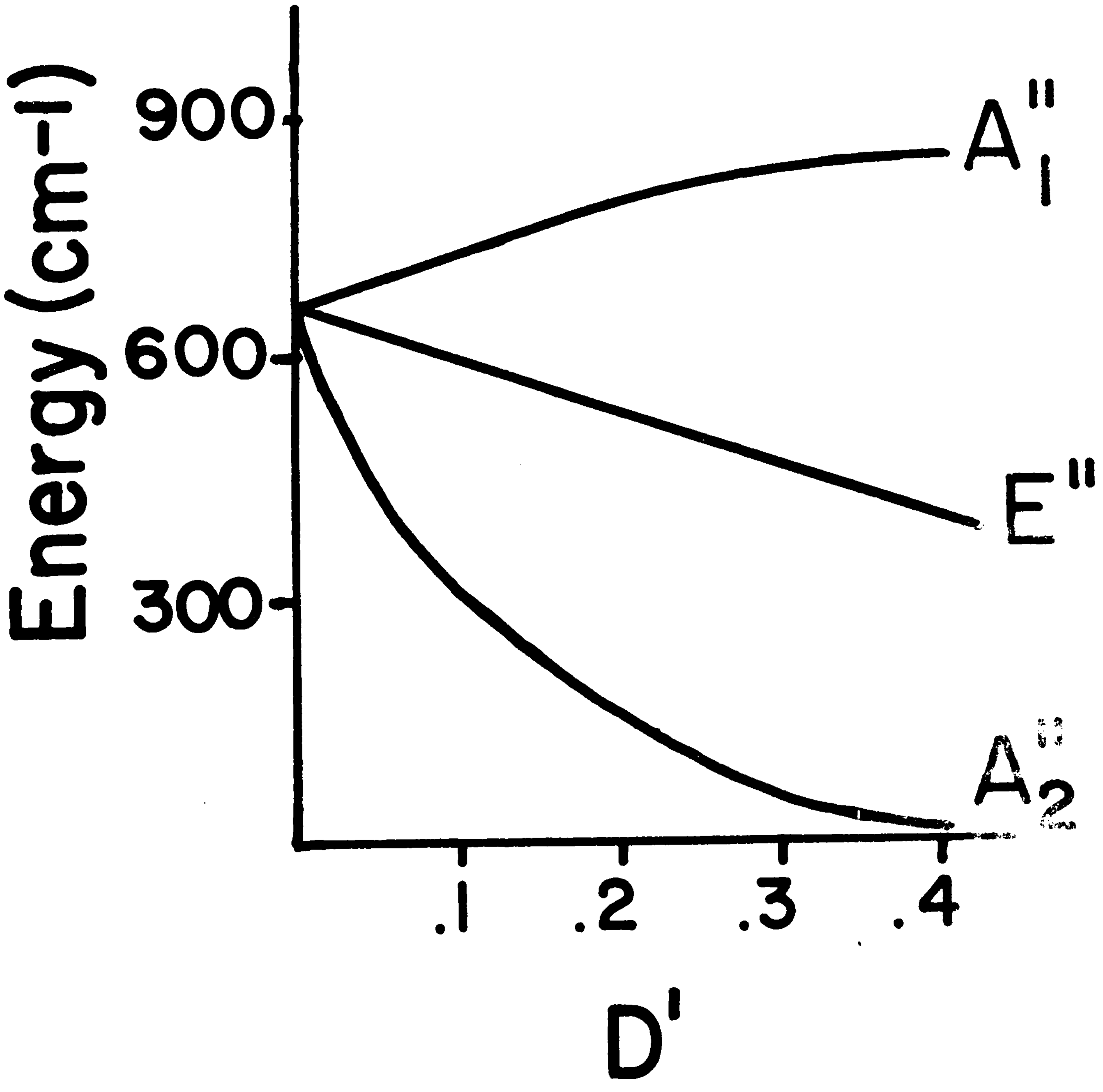

FIGURE 10

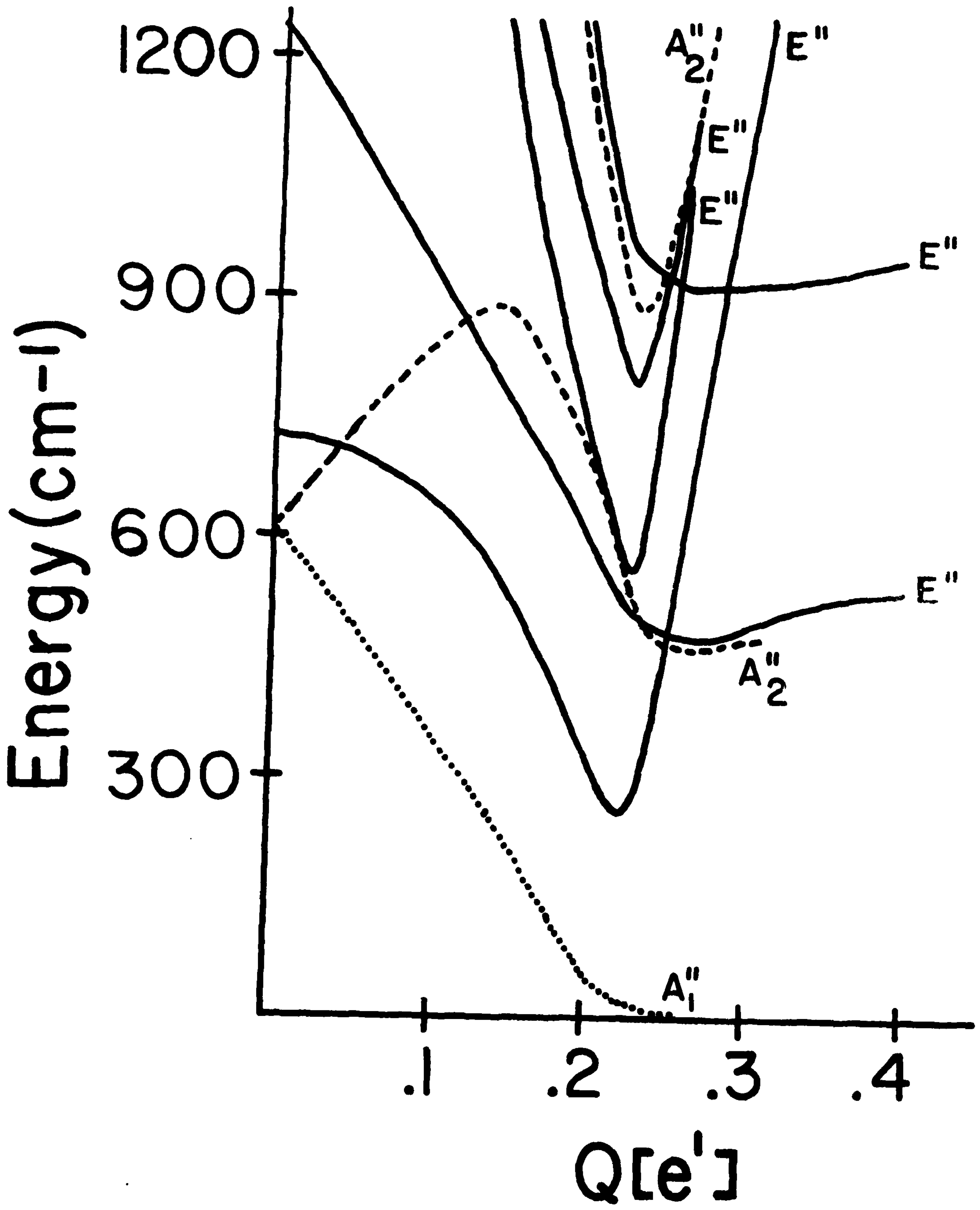

FIGURE 11

TECHNICAL REPORT DISTRIBUTION LIST, GEN

	No. Copies
Office of Naval Research Attn: Code 472 800 North Quincy Street Arlington, Virginia 22217	2
ONR Branch Office Attn: Dr. George Sandoz 536 S. Clark Street Chicago, Illinois 60605	1
ONR Area Office Attn: Scientific Dept. 715 Broadway New York, New York 10003	1
ONR Western Regional Office 1030 East Green Street Pasadena, California 91106	1
ONR Eastern/Central Regional Office Attn: Dr. L. H. Peebles Building 114, Section D 666 Summer Street Boston, Massachusetts 02210	1
Director, Naval Research Laboratory Attn: Code 6100 Washington, D.C. 20390	1
The Assistant Secretary of the Navy (RE&S) Department of the Navy Room 4E736, Pentagon Washington, D.C. 20350	1
Commander, Naval Air Systems Command Attn: Code 310C (H. Rosenwasser) Department of the Navy Washington, D.C. 20360	1
Defense Technical Information Center Building 5, Cameron Station Alexandria, Virginia 22314	12
Dr. Fred Saalfeld Chemistry Division, Code 6100 Naval Research Laboratory Washington, D.C. 20375	1

	No. Copies
U.S. Army Research Office Attn: CRD-AA-IP P.O. Box 1211 Research Triangle Park, N.C. 27709	1
Naval Ocean Systems Center Attn: Mr. Joe McCartney San Diego, California 92152	1
Naval Weapons Center Attn: Dr. A. B. Amster, Chemistry Division China Lake, California 93555	1
Naval Civil Engineering Laboratory Attn: Dr. R. W. Drisko Port Hueneme, California 93401	1
Department of Physics & Chemistry Naval Postgraduate School Monterey, California 93940	1
Dr. A. L. Slafkosky Scientific Advisor Commandant of the Marine Corps (Code RD-1) Washington, D.C. 20380	1
Office of Naval Research Attn: Dr. Richard S. Miller 800 N. Quincy Street Arlington, Virginia 22217	1
Naval Ship Research and Development Center Attn: Dr. G. Bosmajian, Applied Chemistry Division Annapolis, Maryland 21401	1
Naval Ocean Systems Center Attn: Dr. S. Yamamoto, Marine Sciences Division San Diego, California 91232	1
Mr. John Boyle Materials Branch Naval Ship Engineering Center Philadelphia, Pennsylvania 19112	1

SP482-3/A23

472:GAN:716:ddc
78u472-608

TECHNICAL REPORT DISTRIBUTION LIST, 051A

	No. Copies
Dr. M. A. El-Sayed Department of Chemistry University of California, Los Angeles Los Angeles, California 90024	1
~~Dr. E. R. Bernstein~~ ~~Department of Chemistry~~ ~~Colorado State University~~ ~~Fort Collins, Colorado 80521~~	1
Dr. C. A. Heller Naval Weapons Center Code 6059 China Lake, California 93555	1
Dr. J. R. MacDonald Chemistry Division Naval Research Laboratory Code 6110 Washington, D.C. 20375	1
Dr. G. B. Schuster Chemistry Department University of Illinois Urbana, Illinois 61801	1
Dr. A. Adamson Department of Chemistry University of Southern California Los Angeles, California 90007	1
Dr. M. S. Wrighton Department of Chemistry Massachusetts Institute of Technology Cambridge, Massachusetts 02139	1

	No. Copies
Dr. M. Rauhut Chemical Research Division American Cyanamid Company Bound Brook, New Jersey 08805	1
Dr. J. I. Zink Department of Chemistry University of California, Los Angeles Los Angeles, California 90024	1
Dr. D. Haarer IBM San Jose Research Center 5600 Cottle Road San Jose, California 95143	1
Dr. John Cooper Code 6130 Naval Research Laboratory Washington, D.C. 20375	1
Dr. William M. Jackson Department of Chemistry Howard University Washington, DC 20059	1
Dr. George E. Walraffen Department of Chemistry Howard University Washington, DC 20059	1
Dr. Rudolph J. Marcus Office of Naval Research Scientific Liaison Group American Embassy APO San Francisco 96503	1
Mr. James Kelley DTNSRDC Code 2803 Annapolis, Maryland 21402	1